Recent Progress on Metal Halide Perovskite Solar Minimodules

Zhichun Yang[1], Zonghao Liu[1], Vahid Ahmadi[2], Wei Chen[1], Yabing Qi*[3]*

[1] Wuhan National Laboratory for Optoelectronics (WNLO), Huazhong University of Science and Technology (HUST), Wuhan, China

[2] Department of Electronics, Tarbiat Modares University, P.O. Box 14115-194, Tehran, Iran

[3] Energy Materials and Surface Sciences Unit (EMSSU), Okinawa Institute of Science and Technology Graduate University (OIST), 1919-1 Tancha, Onna-son, Kunigami-gun, Okinawa 904-0495, Japan

*Corresponding authors and E-mails:

Zonghao Liu, E-mail: liuzonghao@hust.edu.cn; Yabing Qi, E-mail: Yabing.Qi@OIST.jp

Keywords: perovskite solar cells, minimodule, efficiency, stability

The rapid development of perovskite solar cells (PSCs) in view of efficiency during the past decade has made this emerging photovoltaic (PV) technology a promising competitor in the PV market. In the next step, PSCs need be manufactured into module scale to meet the commercialization requirements for further practical application. Demonstrations of perovskite solar modules (PSMs) and their improvements in efficiency and stability have recently become an intense area of research activities. Minimodules with the size suitable for laboratory investigation are naturally recognized as a desirable model for the study of PSMs. Herein, we review the recent progress and challenges in perovskite minimodules and the efforts to improve their scalable fabrication, efficiency and stability. We will also discuss minimodule architectures, minimodule fabrication and progress in the scalable deposition of perovskite and charge-transport layers as well as minimodule encapsulation.

1. Introduction

Perovskite solar cells (PSCs) have drawn tremendous attention in the photovoltaic (PV) research community because of their high efficiency, low cost and easy fabrication.[1] In the

past decade, the efficiency of small-size PSCs with an active area of ~ 0.1 cm^2 has skyrocketed to a prominent power conversion efficiency (PCE) of 25.5%, which is comparable to other kinds of thin film photovoltaics.[2] Nevertheless, PSCs are still facing issues, in particular the scalable fabrication of PSCs into module scale and their long-term operational stability.

Due to the difficulty of directly applying the approaches in the fabrication of PSCs to perovskite solar modules (PSMs), the efficiencies of PSMs are much inferior to other kinds of commercialized solar modules.[3] **Figure 1**a shows the remarkable progress of PSCs and PSMs with different sizes, and Figure 1b shows the evolution of PCE records for different types of solar cells at different size scales. The PCE record of perovskite minimodules (< 200 cm^2) is 20.1% with a designated illumination area of 63.98 cm^2, 12 serial cells, manufactured by Utmolight.[4] The PCE record of submodules for PSMs is 17.9% with a designated illumination area of 802 cm^2, 55 series cells, manufactured by Panasonic.[4] Clearly, the efficiencies of PSMs are still substantially lower than other kinds of commercialized solar modules.[4] To facilitate the development of PSCs, demonstrations of PSMs and their improvements in efficiency and stability have recently become an intense area of research activities.

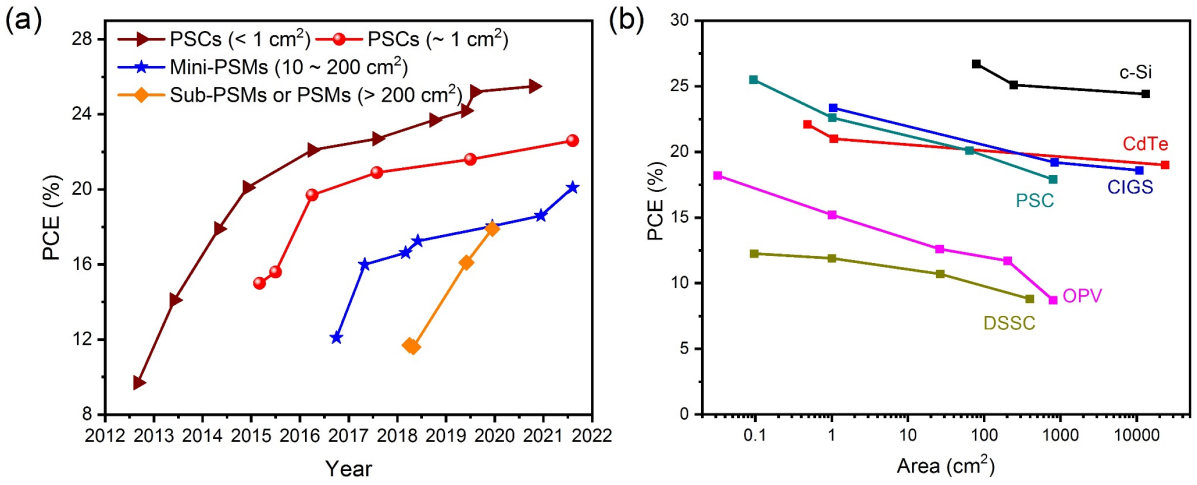

Figure 1. a) The remarkable progress in PCE of PSCs and PSMs with different sizes. b) The PCE records evolution of different types of solar cells at various size scales.

To date, most of the reported PSMs are in the form of minimodules. Despite a relatively

smaller size, perovskite minimodules can still act as a superb model for the study of PSMs to facilitate the development of this emerging PV technology. In this context, we will review the recent progress and challenges in perovskite minimodules, including the related efforts devoted to improving their scalable fabrication, efficiency, and stability. Then, we discuss the architectures of PSMs, PSMs fabrication, and the progress in the scalable deposition of perovskite and charge-transport layers as well as module encapsulation.

2. PSM architecture

In general, PSMs have similar functional layers as PSCs, including transparent conductive oxide (TCO) substrate, charge (electron and hole) transport layers, perovskite layer and metal electrode.[5] PSCs are usually fabricated in the form of single cells. However, it is impractical to construct PSMs in the same form as PSCs due to the non-negligible sheet resistance increase of TCO across a long distance. To minimize the resistance loss, PSMs can be fabricated by connecting the isolated adjacent subcells in series or parallel to form a module as shown in **Figure 2**.[6]

Since 2016 Martin A. Green and the co-workers have been compiling the efficiency of perovskite solar minimodule in "Solar cell efficiency tables (version 49)",[7] and numerous advances have been achieved to address the scientific and technical challenges for the development of highly efficient and stable PSMs. Typically, the most significant challenge is how to reduce the efficiency loss when the device area increases from a cell level to the minimodule, or even submodule and module scale. The efficiency difference between the small-area device and the large-area module is generally attributed to the following aspects: (1) the increase of series resistance of the TCO substrate resulting inferior module current and fill factor; (2) the decreased shunt resistance of the module device from the non-uniform coating of perovskite layer and other interface layers over large scale; (3) the non-ideal contact and unavoidable dead area for the interconnection of subcells to a module fabrication.[8] Currently,

the main module interconnection fabrications are series and parallel interconnection.

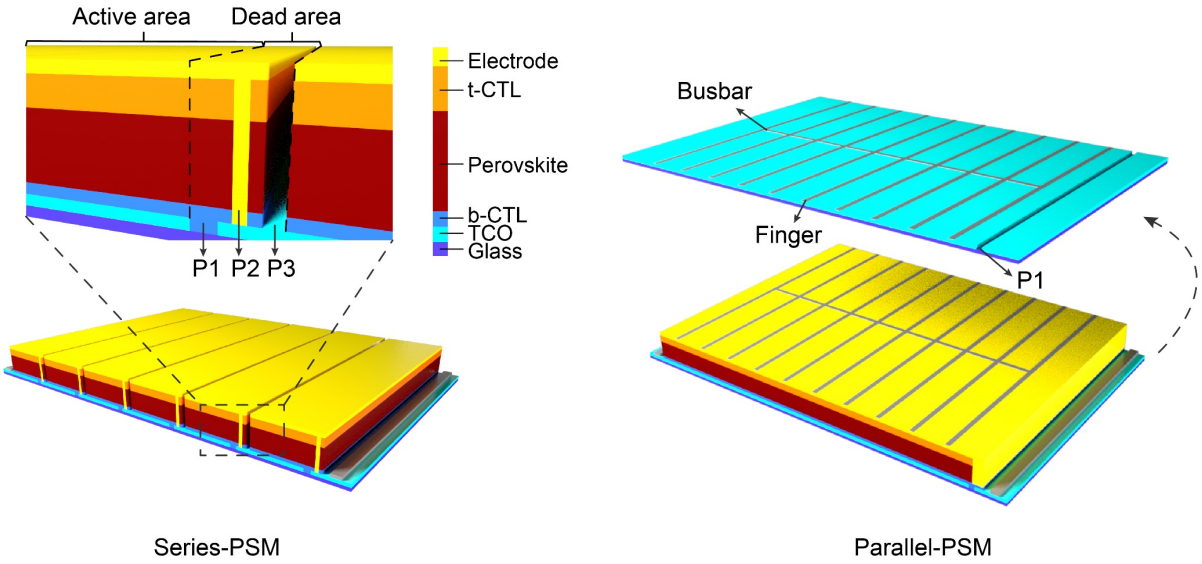

Figure 2. Schematic diagrams of series- and parallel-connected PSMs.

2.1 Series module

To date, most of the reported PSMs are based on a series design, in which the device is divided into several stripe-shaped subcells. Neighboring subcells are connected through interconnections, which consist of P1, P2, and P3 lines.[9] These three lines should be parallel to each other to avoid unwanted cross-talking. It should be noted that the P1-P2-P3 interconnection regions are described as "dead areas", *i.e.*, inactive areas. To improve the power generation in the given module area, the P1-P2-P3 interconnection regions should be minimized to improve the ratio of the active area *versus* the total area. This ratio is defined as the geometric fill factor (GFF), and it can be calculated as GFF = sum of active area / total area. However, a proper safe distance between the three lines with a suitable width of each line is also important to avoid undesirable electric leakage or loss. In PSMs based on the series configuration, P1 lines are generally scribed on TCO substrate to isolate adjacent subcells before the deposition of charge-transport layers and perovskite layer. After the deposition of charge-transport layers and perovskite layer, P2 lines are scribed from the top of charge (electron or hole) transport layer/perovskite/charge (hole or electron) transport layer down to the underlying TCO substrate

without significantly destroying the latter. Because P2 lines are the channels scribed to form electrical connection in series from the top contact of one subcell to the bottom contact of the adjacent subcell after the deposition of the top electrode, it is important to achieve clean P2 lines with a suitable width to guarantee good Ohmic contact between the top electrode and TCO substrates. In some cases, the bottom charge transport layer on the TCO substrate in the P2 channel is allowed due to the limited resistance loss when using ultrathin charge transport layers with high conductivity.[10-12] P3 lines are scribed on the top contact electrode to isolate neighboring subcells. Furthermore, the width of each subcell, *i.e.* the distance between two neighboring P1 lines also affects the charge transport length across the subcell. A suitable module pattern design is important for high-efficiency PSMs due to the limited conductivity of TCOs.[13] Laser and mechanical scribing approaches have been reported for manufacturing P1-P2-P3 interconnections in PSMs. To obtain high-quality P1-P2-P3 interconnections, laser scribing is recommended because of its fast production rate, high production rate, high resolution, and high selectivity.[14-16] Since laser scribing is based on the interaction between the laser and matter, the selection of suitable laser scribing parameters is important to achieve high-quality interconnections.[17, 18] In the case of fabricating flexible PSMs on a plastic substrate, it is extremely important to optimize the laser parameters, the so-called "cold processing" femtosecond laser system is the best choice due to its high selectivity and high precision for interconnection processing. In addition to line interconnections contact, Rakocevic and coauthors recently demonstrated that point contact interconnections design is a promising design to decrease the interconnections losses from 5% to 1%, giving GFFs of up to 99 %.[19]

Besides, the module architecture also affects device stability. In PSMs based on the series configuration, perovskite is directly in contact with the metal electrode at the P2 lines. Such a contact poses a big concern for the long-term stability of series modules due to easy lateral

interdiffusion of metal and/or the reaction between perovskite and metal electrode.[20] In P3 lines, the active layer is directly exposed, which can be the channels for the outward release of perovskite decomposition by-products or H_2O/O_2 ingress.[12] Suitable barrier or encapsulation at interconnections is recommended to retard such issues (**Figure 3**).[12, 20]

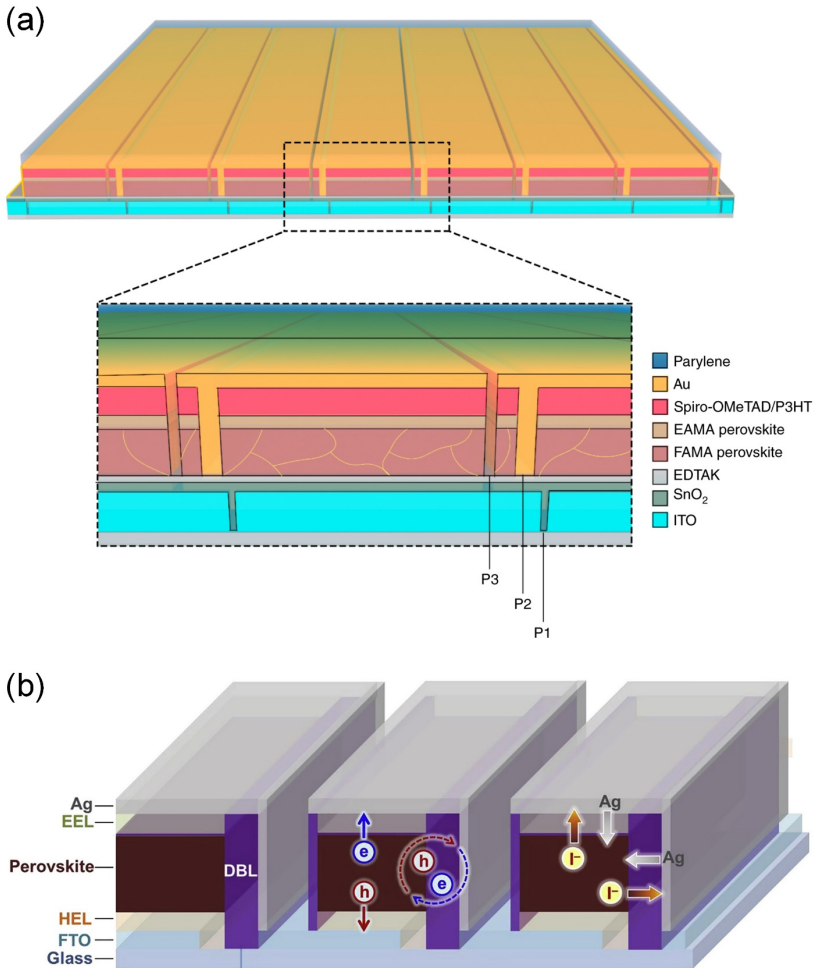

Figure 3. a) Schematic illustration of a holistic interface strategy consisting of four treatments for the functional layers and their interfaces within a perovskite solar minimodule. Reproduced with permission.[13] Copyright 2020, Springer Nature. b) Schematic illustration of diffusion barriers within a perovskite minimodule. Reproduced with permission.[20] Copyright 2019, Elsevier.

2.2 Parallel module

Besides series PSM, parallel PSM with a grid-connected design is an alternative

architecture option. In parallel PSMs, the adjacent subcells are connected in parallel by metal grids, which are added to the top electrode and/or bottom TCO electrode of the device (Figure 2b). The grids normally consist of several fine parallel lines called "fingers" crossed by a few thicker fingers that collect current from the fingers to the busbars. Because this approach typically has many parallel connections, it generally exhibits better system robustness; for example, if one subcell is broken or partially shaded and not generating current, the module is still functional. In general, grid-connected modules can also give high GFFs, because grids take up only a small fraction. However, because of the high current generation, more metal/conductor is required to minimize the resistive loss.

At this stage, the development of parallel perovskite solar minimodules slightly lags behind that of series minimodules. This is ascribed to the following challenges: (1) depositing charge-transport layer or the perovskite layer on the TCO/grids substrate with the solution process is very challenging due to a certain thickness of grid lines on the TCO substrate and poor wettability of the precursor solution with metal; (2) the process and material compatibility, the potential reaction of metal grids with the solvents or the deposited charge transport or perovskite materials. To overcome above two challenges, two strategies can be adopted. The first strategy is to bury the grid lines between glass substrate and TCO layer. The second strategy is to deposit the grid lines in the scribed the interconnection channels. Recently, Chen and coauthors fabricated parallel-connected minimodules by depositing Ag grids on fluorine doped tin oxide (FTO) substrate after scribing the deposited perovskite/LiF/C60/BCP layers together with the deposition of metal electrode.[21] As shown in **Figure 4**, the Ag grids are used as a current collector to reduce the sheet resistance of FTO substrate. With this parallel module design, their all-scalable fabricated inverted minimodule with a device structure of FTO/NiMgLiO/$Cs_{0.17}FA_{0.83}PbI_{2.83}Br_{0.17}$/LiF/C60/BCP/Bi/Ag achieved a certified quasi-stabilized efficiency of 16.63% with an active area of 20.77 cm^2. In contrast to the direct contact

of metal electrode with perovskite in series module, such a parallel module design avoids the direct contact of metal electrode/grid with perovskite and allows an adequate space between the grids or electrodes and the active layer. They also adopted Al_2O_3 thin-film encapsulation to further isolate the perovskite or its degradation by-products with metal electrode/grid. The parallel module design is effective to prevent the unexpected contact or corrosive reaction between the metal electrode/grid and perovskite, which is beneficial for the long-term stability of PSMs.

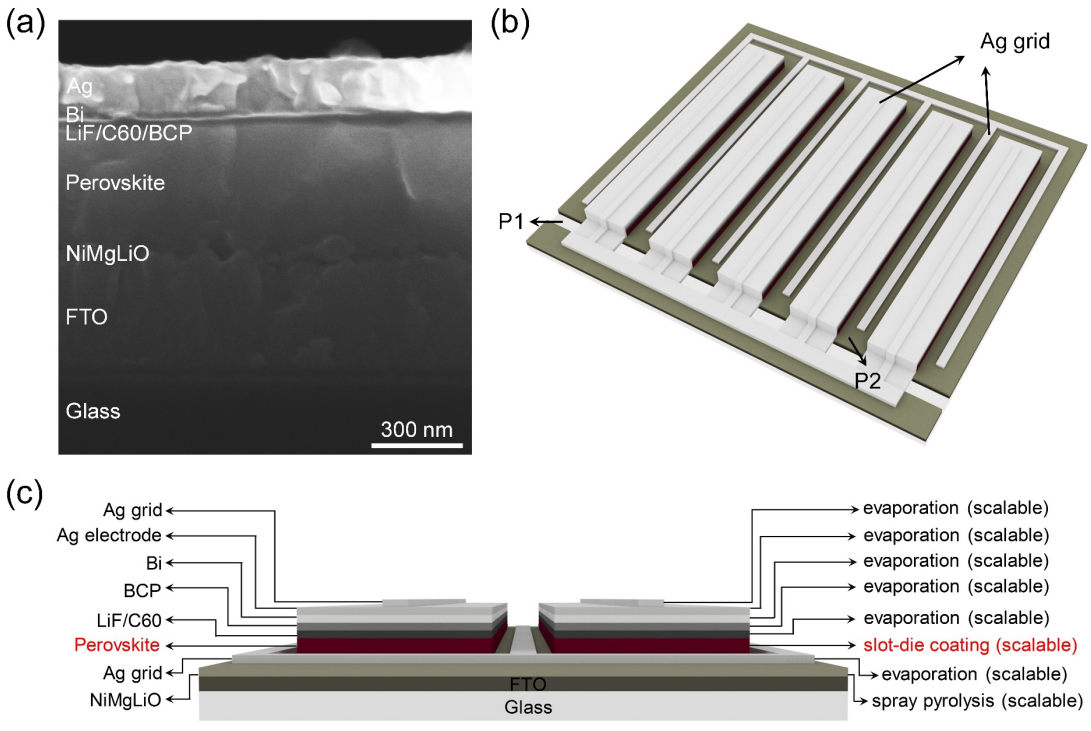

Figure 4. a) High-resolution cross-sectional SEM image of a complete parallel PSM. b) Three-dimensional structure schematic diagram of the designed module connected in parallel. c) Cross-sectional schematic illustration of the fabricated module coupled with the deposition methods of the functional layers. Reproduced with permission.[21] Copyright 2021, American Association for the Advancement Science.

In general, series minimodule can generate a high total voltage that is proportional to the number of the subcells, while its photocurrent is limited to that of the individual subcells. In

contrast, parallel minimodules can produce a high total current that is the sum of the subcells and a low photovoltage equal to the individual subcell. In practical application, the module architecture should also be considered regarding partial failure and shading effect. In a series module, the shaded subcells block the photocurrent of the whole module, and will undergo forcing bias generated from other subcells. This can lead to high temperatures and may completely burn the subcells. In contrast, such an effect would be less for parallel modules, because the parallel module could be recognized as a single cell with low voltage. Meanwhile, the partial failure of subcells in series modules would lead to low current, which limits the current of the whole module, while this problem would be alleviated for parallel modules. In general, for either series or parallel minimodule, there are still many issues that should be resolved. On the one hand, with the difficulty of fabricating efficient minimodule, a holistic-scalable fabrication process needs to be developed. [21] On the other hand, robust encapsulation technology should be developed to tackle the big challenge of module stability. Thus, intrinsically stable barrier or encapsulation materials with high barrier capacity and low reactivity of perovskite, and related encapsulation technology need to be developed.[22, 23]

3. Perovskite minimodule efficiencies

3.1 The efficiency evolution of perovskite minimodule

Figure 5 shows the efficiency record evolution of perovskite minimodules in series and the efficiency development of parallel minimodules. Recently, UtmoLight Co., Ltd from China achieved a stabilized series minimodule efficiency of 20.1% with a designated area of 63.98 cm^2.[4, 24] It is the first time that the PCE of a PSM excessed 20%. Microquanta also announced a stabilized efficiency of 20.2% with a designated area of 20 cm^2.[25] Despite fewer reports on the parallel minimodules, significant progress has been achieved. Recently, a certified quasi-stabilized efficiency of 16.63% with an active area of 20.77 cm^2 for a parallel module architecture was achieved by Chen and coworkers.[21] **Table 1** summarizes the reported studies

about the series and parallel minimodules, including the module structure, PCE, open-circuit voltage (V_{OC}), short-circuit current intensity (J_{SC}), number of cells, GFF, device area, the method of depositing perovskite film, and module stability. To facilitate a comparison of PSMs' efficiency fabricated by different research groups, it will be more convenient if each study can report the detailed performance parameters, including total area, active area, active area efficiency, designated area efficiency or aperture area efficiency, and the GFF values.

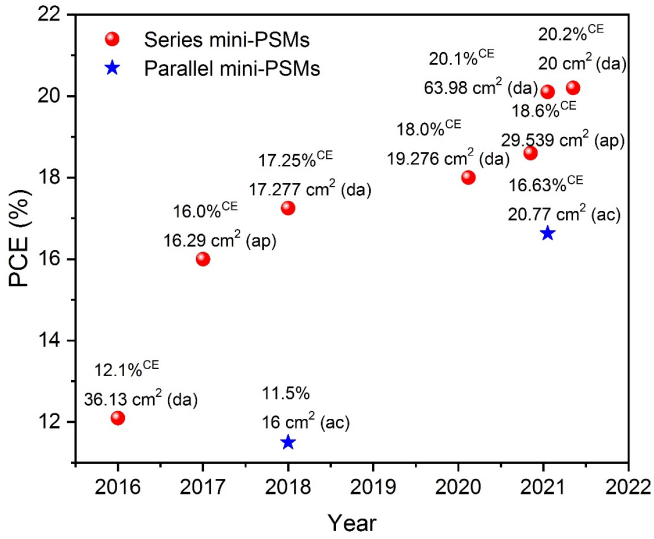

Figure 5. Typical perovskite minimodule efficiency evolution versus year. Abbreviation: ac, active area, ap, aperture area; da, designated area (active area + dead area for interconnections). CE, certified efficiency.

1 **Table 1.** Summary of perovskite solar minimodules connected in series and parallel based on the organic-inorganic perovskites. (> 10 cm^2).

Module structure	PCE (%)	V_{OC} (V)	J_{SC} (mA cm^{-2})	FF (%)	Number of cells	GFF (%)	Area (cm^2)	Perovskite film deposition method	Module stability	Ref.
FTO/c-TiO_2/$MAPbI_3$/spiro-OMeTAD/Ag	14.06[ac]	4.4	~20.8	61.5	4	88	11.09[ac]	Doctor blading	N/A	[26]
ITO/PTAA/$MAPbI_3$/C60/BCP/Cu	14.6[SE]	~17.1	20.3	68.9	16	93.4	57.2[ap]	Doctor blading	Dark, N_2, storage, PSM, T_{100}=480 h	[27]
	15.3[SE]	~18.2	19.5	72.1	17		33.0[ap]			
ITO/PTAA/$MAPbI_3$/C60/BCP/Cu	16.9[ap] (16.4[CE])	18.9	1.18[ap]	75.3	17	93.4	63.7[ap]	Doctor blading	1 Sun equivalent light, MPP, Encapsulated PSM, T_{87}=1000 h	[28]
FTO/c-TiO_2/mp-TiO_2/$MAPbI_3$/spiro-OMeTAD/Au	15.7 [ap] (12.1[CE])	10.5(8.36[CE])	2 [ap] (2[CE])	75.7(71.5[CE])	10	N/A	36.1[ap]	Pressure processing	0.1 Sun UV-filtered, simulated sunlight, 45 °C in ambient air, MPP, Encapsulated PSM, T_{90}=500 h	[29]
ITO/C60/$MAPbI_3$/spiro-OMeTAD/Au	13.98[ac,CE]	14.10	1.14 [ac]	74.45	14	N/A	37.1[ac]	Evaporation/spin coating	N_2, 30 °C, storage, Encapsulated PSM, storage, T_{60}=384 h;	[30]
ITO/C60/$MAPbI_3$/spiro-OMeTAD/Cu	11.09[ac]	13.65	1.07 [ac]	65	14	N/A	37.1[ac]	Evaporation/spin coating	N_2, 30 °C, storage, Encapsulated PSM, storage, T_{90}=720 h;	
ITO/PTAA/$MAPbI_3$/C60/BCP/Cu	18.0[ap] (17.8[SE])	~7	~3.44 [ap]	~74.8	6	93	21.5[ap]	Blade coating	1 Sun equivalent light, 35 °C, Encapsulated PSM, MPP with resistors, T_{90}=400 h	[31]
FTO/SnO_2/3D- $FA_{0.83}Cs_{0.17}PbI_3$/2D-KPF_6/spiro-OMeTAD/Au	19.3%[ac, CE]	6.82	3.76	75.2	6	N/A	17.1[ac]	Slot-die coating	N/A	[32]
FTO/NiMgLiO/$Cs_{0.17}FA_{0.83}PbI_{2.83}Br_{0.17}$/LiF/C60/BCP/Bi/Ag	16.63% [ac, CE]	1.08	~20.6	74.3	8	92.7%	20.77[ac]	Slot-die coating	1 Sun equivalent light, 50 °C, Encapsulated PSMs, MPP tracking, T_{95}=1187 h; Natural day/night recycle, beside the indoor window, connected with	[21]

									a mini-electric fan, T_{97}=10000 h;	
FTO/NiO/$FA_{0.85}MA_{0.15}Pb(I_{0.85}Br_{0.15})_3$/G-PCBM/BCP/Ag	15.6[da] (14.17[CE])	~11.1(10.8[CE])	~1.92[da] (1.84[CE])	~73.2(71.5)	10	N/A	35.8[da]	Slot-die coating	85 °C, RH 85%, Encapsulated PSM, T_{95}=1000 h; 1 Sun with UV filter, 60 °C, Encapsulated PSM, MPP, T_{91}=1000 h;	[20]
FTO/TiO_2/SnO_2/PCBM/$MAPbI_3$/spiro-OMeTAD/Au	18.13[ac]	6.71	3.68[ac]	73.4	6	72	21[ac]	Thermally co-evaporated	1 Sun, N_2, RH 5%, unencapsulated PSM, MPP, T_{90}=100 h; 65 °C, RH 5%, unencapsulated PSM, T_{80}=100 h;	[33]
FTO/SnO_2/C60/$Cs_{0.1}FA_{0.9}PbI_3$/spiro-OMeTAD/Au	9.34[da]	13.55	1.15[da]	59.6	14	90	91.8[da]	HCVD	RH 35%, unencapsulated PSM, storage, T_{95}=1440 h; 1 Sun, N_2, 25 °C, Encapsulated PSM, MPP, T_{80}=500 h	[34]
FTO/c-TiO_2/$Cs_{0.07}FA_{0.93}PbI_3$/spiro-OMeTAD/Au	14.6[ac]	5.84	3.67[ac]	68.1	6	N/A	12[ac]	HCVD	1 Sun, RH 60%, unencapsulated PSC, MPP, T_{56}=1000 min;	[35]
ITO/PTAA/$FA_{0.92}Cs_{0.08}PbI_3$/C60/BCP/Cu	18.6%[ap,CE]	8.72	2.83	75.41	17	~92%	29.5[ap]	Blade coating	1 Sun, N_2, RH 5%, unencapsulated PSC, MPP, T_{100}=1200 min 1 Sun, 50 ± 5 °C, encapsulated PSMs MPP, $T_{93.6}$=1056 h	[36]
FTO/c-TiO_2/$FAPb(I_{0.85}Br_{0.15})_3$/spiro-OMeTAD/Au	14.7[ac]	6.29	3.55[ac]	66	6	N/A	12[ac]	HCVD	Dark, N_2, unencapsulated PSM, storage, $T_{96.4}$=3600 h; 1 Sun, N_2, RH 5%, unencapsulated PSC, MPP, T_{80}=535 h;	[37]
FTO/SnO_2/$Cs_xFA_{1-x}PbI_{3-y}Br_y$/spiro-OMeTAD/Au	12.24[ac]	9.18	2.25[ac]	52.8	9	N/A	41.25[ac]	HCVD	1 Sun, N_2, RH 5%, unencapsulated PSM, MPP, T_{80}=388 h	[38]
									30 °C, RH 30%, unencapsulated PSM, storage, T_{83}=200 h;	

									60 °C, RH 30%, unencapsulated PSM, storage, T_{80}=200 h;	
FTO/c-TiO_2/mp-TiO_2/$MAPbI_{3-x}Cl_x$/spiro-OMeTAD/Au	15.3[ac]	6.65	3.66[ac]	63.0	6	N/A	12[ac]	Gas-solid process	N/A	[39]
FTO/SnO_2/$(FA_{0.85}MA_{0.15})_{0.95}Pb(I_{0.85}Br_{0.15})_3$/spiro-OMeTAD/Au	13.9[ac]	13.38	1.66[ac]	62.0	12	N/A	53.6[ap]	Spin coating/Solvent bath process	N/A	[40]
PET/ITO/SnO_2/$Cs_{0.05}(FA_{0.85}MA_{0.15})_{0.95}Pb(I_{0.85}Br_{0.15})_3$/ spiro-OMeTAD/Au	15.2[ap]	6.727	3.28[ac]	69	6	N/A	16.07[ap]	Spin coating/antisolvent	Dark, RH 20%, unencapsulated PSM, storage, T_{80}=1000 h;	[41]
FTO/c-TiO_2/mp-TiO_2 /$(FAPbI_3)_{0.95}(MAPbBr_3)_{0.05}$ /WBH/P3HT/Au	17.1[da]	8.78	2.72[da]	71.7	8	94.4	24.97[da]	Spin-coating	N/A	[42]
FTO/c-TiO_2/mp-TiO_2 /$(FAPbI_3)_{0.95}(MAPbBr_3)_{0.05}$ /WBH/P3HT/Au	17.1[da]	8.66	2.72[da]	72.6	8	94.4	24.97[da]	Bar-coating	N/A	[42]
FTO/SnO_2/ $(CsPbI_3)_{0.05}((FAPbI_3)_{1-x}(MAPbBr_3)_x)_{0.95}$/spiro-OMeTAD/Au	17.88[CE,ap]	7.52	3.02[da]	78.6	7	90.8	25.49[ap]	Spin coating	Dark, storage, Encapsulated PSM, T_{90}=5040 h;	[43]
SnO_2-EDTAK/$Cs_{0.05}FA_{0.54}MA_{0.41}Pb(I_{0.98}Br_{0.02})_3$/spiro-OMeTAD-P3HT/Au	16.6[da]	7.64	2.99[da]	72.9	7	91	22.4[da]	Spin coating	1 Sun, N_2, 40 °C, Encapsulated PSM, MPP, T_{90}=1570 h, T_{80}=2680 h; RH 5%, 60 °C, Encapsulated PSM, T_{80}=1000 h	[12]
FTO/c-TiO_2/mp-TiO_2/Graphene/$MAPbI_3$/spiro-OMeTAD/Au	12.6[ac]	8.57	2.27[ac]	64.6	8	N/A	50.6[ac]	Spin coating/Doctor blading	ISOS-D-1, PSM, storage, T_{80}=1630 h	[44]
FTO/c-TiO_2/mp-TiO_2/Graphene/$(Cs_{0.01}FA_{0.79}MA_{0.15})Pb(I_{0.85}Br_{0.15})_3$/$MoS_2$/spiro-OMeTAD/Au	15.3[ac] (13.4)	10.46	2.20[ac]	65.1	10 (22)	N/A	82[ac] (108[ac])	Spin coating	ISOS-D-2, 65 °C, PSM, T_{80}=400 h	[45]
FTO/SnO_2/$MAPbI_3$/spiro-OMeTAD/Au	12.03[da]	5.80	3.38[da]	61.3	6	91	22.4[da]	Spin coating	1 Sun, N_2, unencapsulated PSM, MPP, T_{80}=515 h	[11]
FTO/c-TiO_2/(m-TiO_2/m-ZrO_2/m-C)/$(5\text{-AVA})_x(MA)_{1-x}PbI_3$	10.5[ac]	3.72	19.6	57.6	4	N/A	31[ac]	Screen-printing/drop-diffusion	Ambient Air, RH 65%, storage, unencapsulated PSM, T_{95}=2000 h;	[46]

									White light LED, unencapsulated PSM, MPP, T_{96}=72 h	
	10.7 [ac]	9.6	17.7	62.9	10	N/A	70 [ac]	Screen-printing/ drop-diffusion	–	
FTO/c-TiO_2/(m-TiO_2/m-ZrO_2/m-C)/(5-AVA)$_x$(MA)$_{1-x}$$PbI_3$	10.4 [ac]	9.3	2 [ac]	56	10	N/A	49 [ac]	Screen-printing/ drop-diffusion	1 sun, 25 °C, RH 54%, unencapsulated PSM, MPP, T_{100}=1000 h; Outdoor, 30 °C, RH 80%, encapsulated PSM, T_{100}=720 h; RH 54%, unencapsulated PSM, storage, T_{100}=8760 h	[47]
FTO/c-TiO_2/(m-TiO_2/m-ZrO_2/m-Carbon)/(5-AVA)$_x$(MA)$_{1-x}$$PbI_3$	11.2[ac]	7.1	2.2 [ac]	70.4	8	46.7	46.7[ac]	Screen-printing/ drop-diffusion	1 sun, 55 °C, short circuit, PSM, T_{100}=10,000 h	[48]

Abbreviation: ac, active area, ap, aperture area; da, designated area (active area + dead area for interconnections). CE, certified efficiency; ITO, indium tin oxide; FTO, fluorine doped tin oxide; c-TiO_2, compact TiO_2; mp, mesoporous TiO_2; spiro-OMeTAD, 2,2',7,7'-tetrakis(N,N-di-4-methoxyphenylamino)-9,9'-spirobifluorene; PCBM, [6,6]-phenyl-C60,61 butyric acid methyl ester; PTAA, poly[bis(4-phenyl)(2,4,6-trimethylphenyl)amine]; PEDOT:PSS, poly(3,4-ethylenedioxythiophene):poly(styrenesulfonate); P3HT, poly(3-hexylthiophene-2,5-diyl) regioregular; 5-AVA, 5-aminovaleric acid. The device performance values are mainly obtained from current-voltage curves.

3.2 Recommendations for minimodule efficiency test

Standard module efficiency test process is important for obtaining accurate efficiency values. Module performance measurement proposal,[49] photovoltaic calibrations at the national renewable energy laboratory (NREL) and uncertainty analysis following the ISO 17025 guidelines can be suggested for the certification of solar modules, and the measurement procedure is shown in **Figure 6**.[50] Currently, because the specific measurement standard has not been defined, the certification of PSMs can also be performed according to the above proposal. Beyond that, the special hysteresis behavior of the perovskite module cannot be effectively evaluated yet and sometimes the existence of hysteresis leads to the uncertainty of PSM performance evaluation. For this issue, the quasi- or steady state measurements for PSMs are recommended. In other words, it is exigent to establish the proposals to evaluate accurately the device performance of PSCs and PSMs.

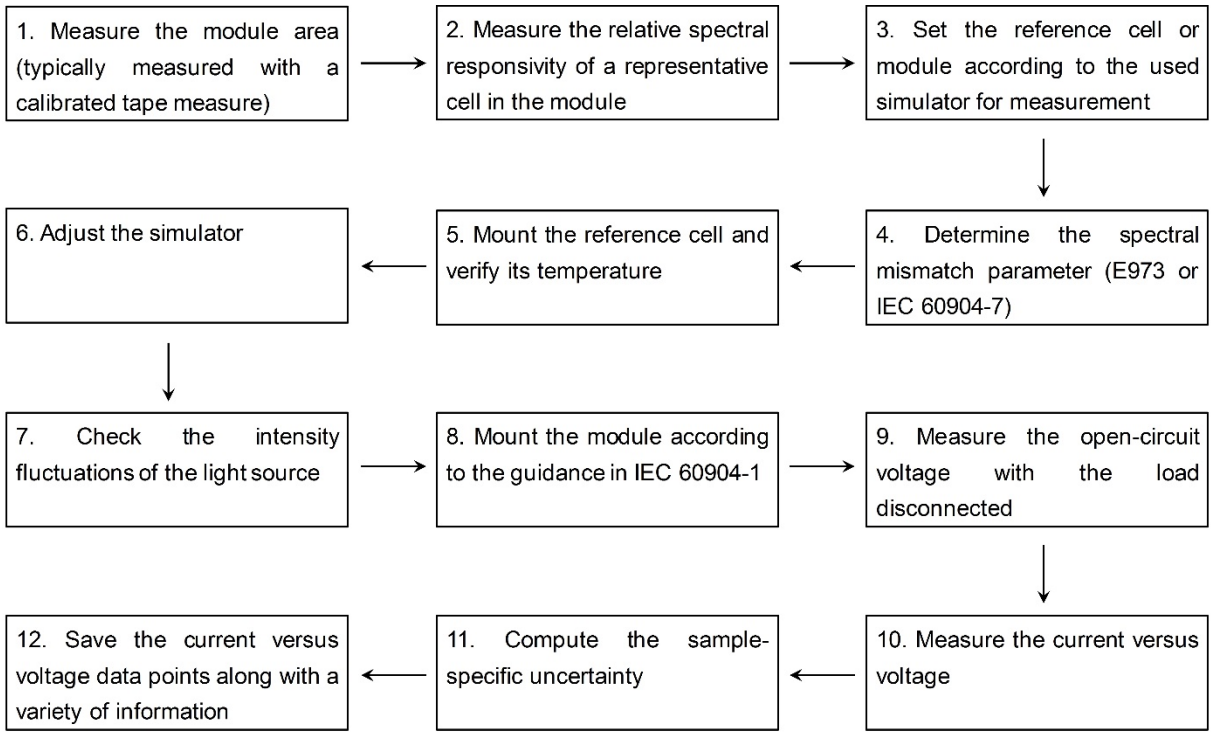

Figure 6. Procedures of the module measurement proposed by NREL following the ISO 17025 guidelines, reproduced according to Ref 50.[50]

3.3 Efficiency improvement strategies for minimodule

Based on the discussion above, one of the most urgent tasks for promoting the commercialization of this emerging PV technology is to reduce the efficiency gap between the mini-/submodules and small-area PSCs. The main efficiency loss can be ascribed to the optical and electrical loss during the device area enlargement process. In detail, regarding the optical loss, the inevitable laser scribed interconnection channel leads to the reduction of effective light absorbing area and the non-uniformity of perovskite layer as well as other functional layers when increasing the area results in inferior device performance. Furthermore, the electrical loss attributes to the increase of sheet resistance of TCO substrates and the interconnection contact resistance loss. In addition, the defect induced recombination loss mainly from the critical perovskite layer is also an important electrical loss source. Thus, on the one hand, the technology development of fabricating uniform, high-quality and defect-less perovskite films as well as other interface films is the most important aspect and improving the GFF of min-/submodule by improving the laser pattern capability is also a critical direction. On the other hand, it is essential to optimize the module structure and develop effective grid or finger schemes to improve the carrier collection efficiency and reduce the performance loss from the increase of sheet resistance and optimize the interconnection towards ohmic contact to reduce the contact resistance between the subcells.

4. Perovskite minimodule fabrication

4.1 Perovskite film deposition

As for fabricating a perovskite minimodule, the most important and challenging issue is the deposition of high-quality perovskite film over a large area. At present, the commonly reported methods to deposit perovskite films are spin coating,[39] doctor blading,[26, 31] slot-die coating,[21, 51] spray coating,[52, 53] and vapor-based methods.[54]

4.1.1 Spin coating

Spin coating is the most commonly used method to deposit high-quality perovskite films

for the fabrication of efficient PSCs and minimodules. Generally, it can be divided into the "one-step" and "two-step" methods as shown in **Figure 7**.

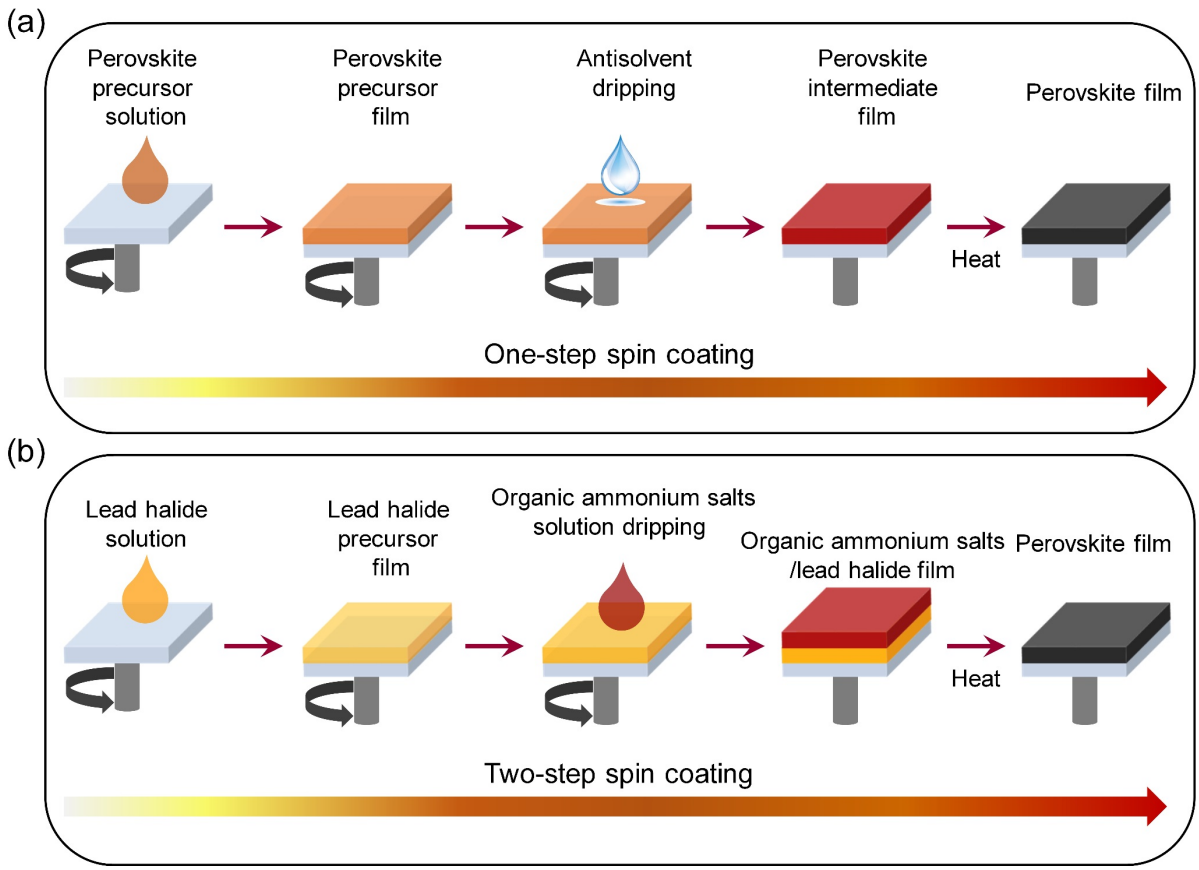

Figure 7. Schematic illustration of a) "one-step" and b) "two-step" spin coating method for the deposition of perovskite films for perovskite solar minimodule.

In the "one-step" spin coating method, the perovskite precursor species are firstly dissolved in the commonly used polar aprotic solvents such as N, N-dimethylformamide (DMF), dimethyl sulfoxide (DMSO), N-methyl-2-pyrrolidone (NMP), or γ-butyrolactone (GBL) to form a precursor solution.[55] Then, the prepared solution is spin-coated on the pre-treated substrate and the solvents can be rapidly removed by the centrifugal force during the spin coating process at high speed. To control the film quality, anti-solvent treatment is commonly used to assist the formation of a high-quality perovskite intermediate film. Then, a fully crystallized perovskite film can be obtained after thermal annealing.

Although the perovskite films of those reported highest performance lab-scale PSCs are almost all fabricated by spin coating,[56] as device area increases it is increasingly challenging to ensure perovskite film uniformity from the center to edge.[57] To solve this problem, Huang and coauthors reported a simple dynamic antisolvent quenching (DAS) process for spin coating large-area perovskite films. In their DAS process, antisolvent is continuously dropped from the center to the edge by moving the pipette, such a DAS process allows antisolvent to interact with the whole precursor wet film resulting in simultaneously homogenous nucleation. The homogeneity of the film from the center to the edge can be greatly enhanced via a DAS process (**Figure 8**).[57] The minimodule with a device structure of FTO/SnO_2/Perovskite/spiro-OMeTAD/Au achieved a certified efficiency of 17.4% with an aperture area of 53.64 cm^2. The dropping of antisolvent was also optimized by using a multi-tip pipette to fabricate large-area perovskite films for minimodule fabrication.[58]

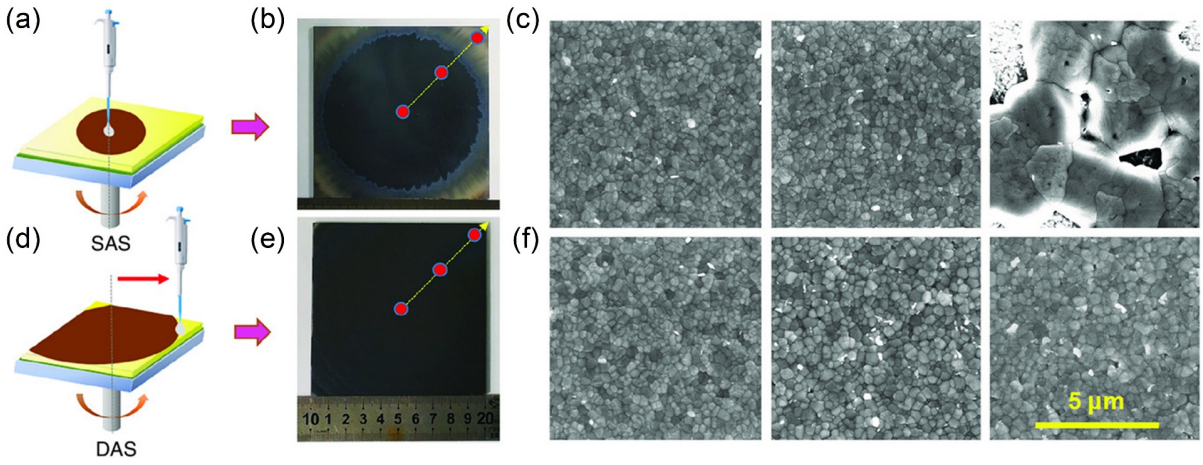

Figure 8. a) Schematic diagram of the SAS process and b) the photograph of a large 10 × 10 cm^2 perovskite film deposited using the SAS process. c) From left to right, the SEM images correspond to the center to edge of the large 10 × 10 cm^2 perovskite film deposited using the SAS process. d) Schematic diagram of the DAS process and e) the photograph of a large 10 × 10 cm^2 perovskite film deposited using the DAS process. f) From left to right, the SEM images correspond to the center to edge of the large 10 × 10 cm^2 perovskite film deposited using the

DAS process. Reproduced with permission.[57] Copyright 2019, Wiley-VCH.

Besides one-step spin coating, the "two-step" spin coating method commonly used for fabricating high efficiency lab-scale PSCs[59-61] has also been used to fabricate minimodules.[12, 43] In this method, an inorganic lead halide solution is firstly deposited to form a solid film. Then, the organic ammonium halide/isopropanol (IPA) solution is spin-coated on the top of the deposited lead halide film, and the perovskite film is formed by the interdiffusion process. The fully crystalized perovskite film is formed after thermal annealing. In general, it is easy to obtain a high-quality lead halide solid-state film by spin coating. Because of the high concentration of organic ammonium halide/isopropanol (IPA) solution as well as the fast evaporation rate of IPA, it is important to achieve uniform spreading out of the organic ammonium halide solution over a large area during the spin coating process of the organic ammonium solution to deposit high-quality large-area perovskite films.[12] Based on this method, Qi and co-authors fabricated large-area $Cs_{0.05}FA_{0.54}MA_{0.41}Pb(I_{0.98}Br_{0.02})_3$ film on 5 cm × 5 cm and 10 cm × 10 cm substrates, their n-i-p minimodules achieved an efficiency of 16.6% with an aperture area of 22.4 cm^2.[12] Similarly, Zhao and coauthors reported a minimodule with a certified efficiency of 17.88% on an aperture area of 24.59 cm^2 by composition engineering based on a perovskite composition of $(CsPbI_3)_{0.05}((FAPbI_3)_{1-x}(MAPbBr_3)_x)_{0.95}$.[43]

In the above-mentioned studies, spin coating has been demonstrated to fabricate high-quality perovskite films for efficient minimodules. However, it is difficult to employ spin coating to fabricate high-efficiency PSMs with even larger areas. This is because the wet precursor films rely on the continuous centrifugal force during spinning, and it is difficult to ensure uniformity at the submodule and module scale. This makes the application of spin-coating generally limited to a substrate with a size not larger than 10 cm × 10 cm. Besides, a large portion (over 90%) of the precursor solution is wasted during the spin coating process, which increases the material cost. In short, spin-coating is suitable for the pilot study of

perovskite minimodules, but cannot be easily employed in the practical manufacture of PSMs for mass production. Developing scalable perovskite deposition is essential for the future development of PSMs.

4.1.2 Doctor blade coating

Doctor blade coating is a simple, low-cost, and scalable coating method, which is widely used for the fabrication of large-area organic or inorganic films. This method has been successfully used to deposit large-area perovskite films for PSMs. In a doctor blading process, the perovskite precursor solution is firstly spread over the substrate by the blade to form a precursor wet film as shown in **Figure 9**. Then, the wet precursor film is treated by air knife,[62] antisolvent bath[26] or vacuum[63] to produce a perovskite intermediate phase. Finally, a fully crystallized perovskite film is obtained after thermal annealing. In some cases, the fully crystallized perovskite film is achieved by heating the substrate during the doctor blading process.[27] The perovskite film thickness is generally controlled by several factors, including the precursor concentration, surface tension, and viscosity of the precursor ink, the gap between the blade and substrate, and the speed at which the blade moves across the substrate. Doctor blade coating can be transferred to continuous fabrication of roll-to-roll or sheet-to-sheet setups, in which the blade is stationary and flexible substrates on a roller are in motion. In addition, the ink waste is substantially reduced when compared with spin coating, especially in a continuous roll-to-roll deposition.

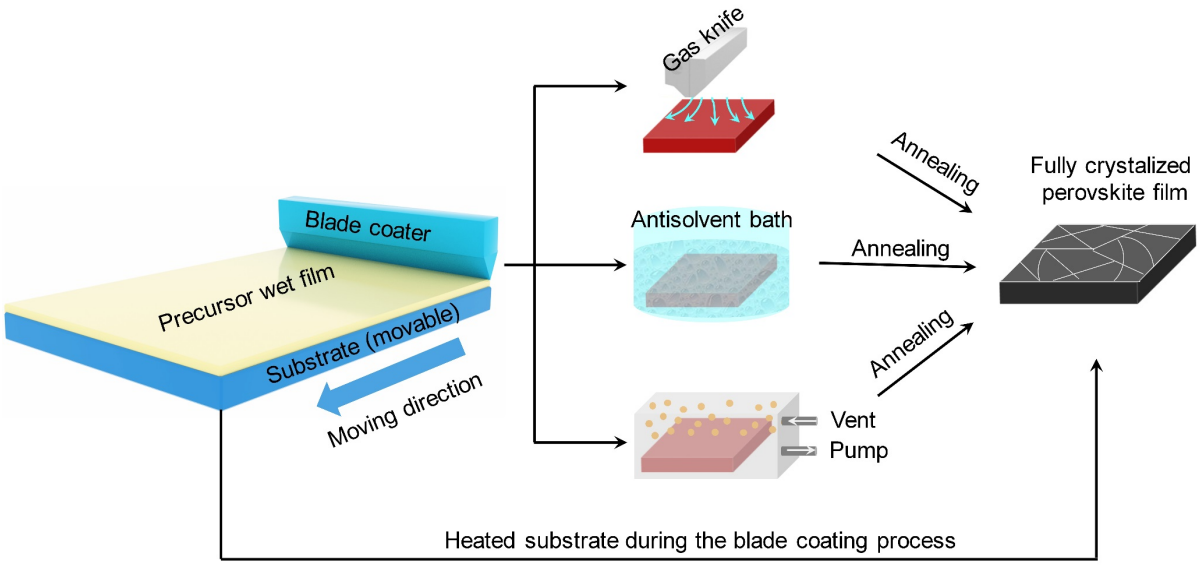

Figure 9. Schematic diagram to illustrate the fabrication process of large-area perovskite films by doctor blade coating together with the post-treatment.

In doctor blade coating, perovskite can be formed with both one and two-step methods. For example, Carlo and coauthors reported the fabrication of $CH_3NH_3PbI_3$ ($MAPbI_3$) perovskite minimodule by the two-step method and achieved an efficiency of 10.4% and 4.3% on areas of 10.1 cm^2 and 100 cm^2, respectively.[64] In their process, PbI_2 was deposited by blade coating and transformed to perovskite by dipping the PbI_2 films into a methylammonium iodide solution. Recently, Huang and coauthors developed a full doctor blade coating method to prepare FA-based perovskites for minimodules.[65] In their process, 4-tert-butylpyridine (TBP) was used as an additive to produce a porous PbI_2 film to facilitate the reaction of PbI_2 with organic ammonium salts to produce perovskite after blade coating of the organic ammonium salts solution. Their minimodule with an aperture area of 10 cm^2 and 53.6 cm^2 gave an efficiency of 16.54% and 13.32%, respectively.[65]

Compared to the two-step method, the one-step method is more widely used. Zhu and coauthors optimized an NMP/DMF solvent system with MACl as an additive to enable wide processing window to produce large-area $MAPbI_3$ films after antisolvent bath and thermal annealing treatment. Their minimodules obtained a stabilized efficiency of 13.3% with an active

area of 11.09 cm^2.[26] Guo and coauthors developed a crystallization strategy with the addition of MACl as an additive and the employment of a vacuum process to deposit large-area $MAPbI_3$ perovskite films via doctor blade coating, giving an efficiency of 11.25% with an active area of 10.08 cm^2.[63] Huang and coauthors conducted a series of studies on blade coating large-area perovskite films for minimodules.[27, 28, 36] They used surfactants to alter the fluid drying dynamics and increase the adhesion of the $MAPbI_3$perovskite ink to the underlying non-wetting poly(bis(4-phenyl)(2,4,6-trimethylphenyl)amine) (PTAA) layer.[27] Their minimodules gave stabilized module efficiencies of 15.3% and 14.6% with aperture areas of 33.0 cm^2 and 57.2 cm^2, respectively.[27] They also fabricated $MAPbI_3$ perovskite film with doctor blading coupled with the designed nitrogen knife quenching process by tailoring solvent coordination capability.[28] They tuned the solvent systems to achieve both fast drying and large perovskite grains at room temperature. Their minimodule achieved a certified module efficiency of 16.4% with an aperture area of 63.7 cm^2.[28] Because the intrinsic instability issue of MA-based perovskites hampers their application in PSCs and PSMs with good stability toward future commercialization,[66] formamidinium (FA) based perovskites with better stability have attracted much attention for highly efficient and stable PSCs as well as PSMs.[67] Recently, Huang and coauthors have developed quick-drying A-B inks, to fabricate large area FA-cesium perovskites for minimodules.[36] In A-ink, $FAPbI_3$ is dissolved in a mixed solvent of 2-ME:ACN, whereas in the B-ink $CsPbI_3$ is dissolved in DMSO. The perovskite minimodules reached a certified stabilized efficiency of 18.6% with an aperture area of ~30 cm^2.[36]

4.1.3 Bar coating

Bar coating is similar to doctor balding, in which a cylindrical bar is used to coat ink on the substrate. The thickness of the bar-coated films can also be tuned by adjusting the gap between the bar and substrate. Similar to doctor blade coating, both the one- and two-step perovskite formation methods can be used in bar coating. For example, Toshiba Corporation

(Tokyo) fabricated a submodule with 703 cm^2 and realized a certified PCE of 11.7% through bar coating by the two-step method.[68] In one-step spin coating, Lewis additive is a successful strategy to produce high-quality perovskite films. Similar to spin coating, Lewis additive also plays an important role in the scalable coating of large-area perovskite films. For example, Park and coauthors developed two Lewis additives, hexamethylphosphoramide (HMPA)[69] and 1,3-dimethyl-3,4,5,6-tetrahydro-2(1H)-pyrimidinone (DMPU)[70] to deposit large-area FACs perovskite films for minimodules (**Figure 10**). Their minimodules gave efficiencies of 17.1% and 17.94% with active areas of 18.66 cm^2 and 19.69 cm^2, respectively. A similar strategy is also adopted in the fabrication of perovskite minimodule via doctor blade coating by Huang and coauthors,[71] indicating the similarity between bar coating and doctor blade coating.

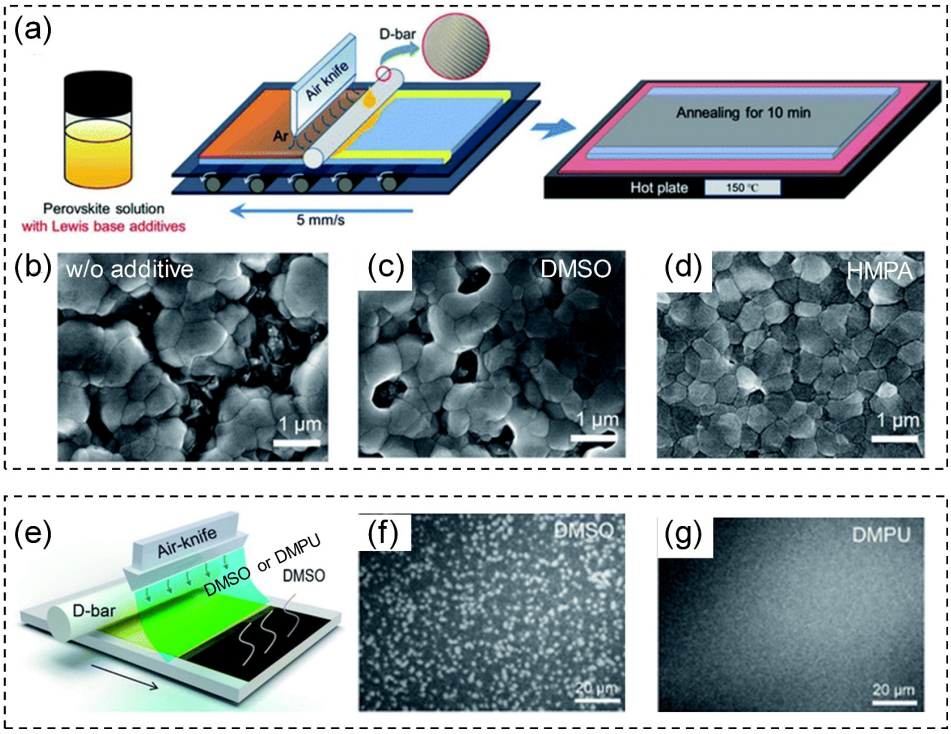

Figure 10. a) Schematic illustration of the bar-coating process for large-area perovskite films. SEM images of the annealed perovskite films prepared b) without a Lewis base additive (pristine) and with c) DMSO and d) HMPA. e) Schematic of the as-deposited (before annealing) films formed by air-knife-assisted bar coating using a DMSO or DMPU-containing perovskite

precursor solution. SEM images of the perovskite film based on f) DMSO and g) DMPU. a) – d) Reproduced with permission.[69] Copyright 2020, Royal Society of Chemistry. e) –g) Reproduced with permission. [70] Copyright 2021, Royal Society of Chemistry.

4.1.4 Slot-die coating

Slot-die coating is another state-of-the-art solution processing technology to deposit high-quality perovskite thin films over large area, which is illustrated in **Figure 11**. It is different from doctor blading on the following aspects: (1) the perovskite ink is reserved in a fluid reservoir; (2) the solution is sequentially squeezed over the substrate by a thin slit during the coating process; (3) the perovskite film thickness can be pre-estimated; (4) it is a contact-free deposition method, which can avoid the direct scratches of the slot-die head on the substrate. The wet precursor film thickness can be adjusted by controlling the precursor solution concentration and viscosity, the gap between the slot-die head and the substrate, the slot-die coating speed, the precursor ink feeding speed, and the pressure of the attached gas knife.

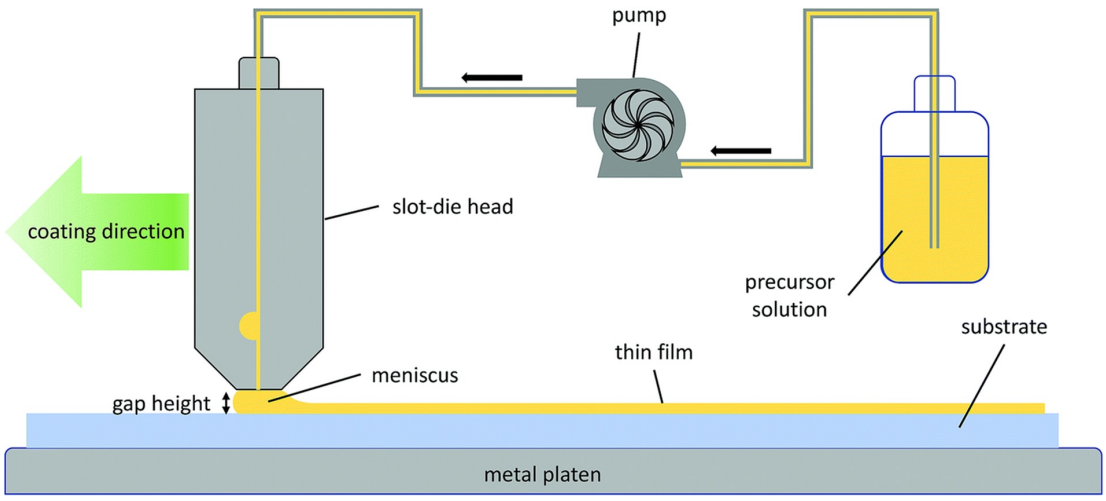

Figure 11. Schematic diagram of slot-die coating large-area perovskite thin films. Reproduced with permission.[51] Copyright 2018, Royal Society of Chemistry.

Fan et al. designed a slot-die coating procedure with vacuum drying processing to fabricate large-area $MAPbI_3$ perovskite films and their 5 × 5 cm^2 minimodule (total active area of 17.3 cm^2) gave an efficiency of 10.6%.[72] As discussed above, FA-based perovskites have attracted

much attention for highly efficient and stable PSMs. It is thus desirable to develop scalable methods to deposit large-area FA-based perovskites. Recently, Chen and coauthors fabricated the formamidinium-cesium (FACs) perovskite films with an area over 200 cm^2 (**Figure 12**a) by slot-die coating. [21] In their method, they improved the precursor wet film stability by using a DMF/NMP system and a room-temperature nonvolatile Lewis base additive of diphenyl sulfoxide. After antisolvent n-hexane bath treatment and thermal annealing, a high-quality fully crystalized FACs perovskite film was obtained (Figure 12b and 12c). This scheme can also produce large-area semi-transparent perovskite films by simply adjusting the precursor concentration (Figure 12d), which is promising for the building integrated photovoltaic (BIPV) application. Recently, Huang and coauthors fabricated large-area perovskite thin film with a size of 20 cm × 20 cm by slot-die coating and achieved a certified efficiency of 19.3% with an active area of 17.1 cm^2.[32]

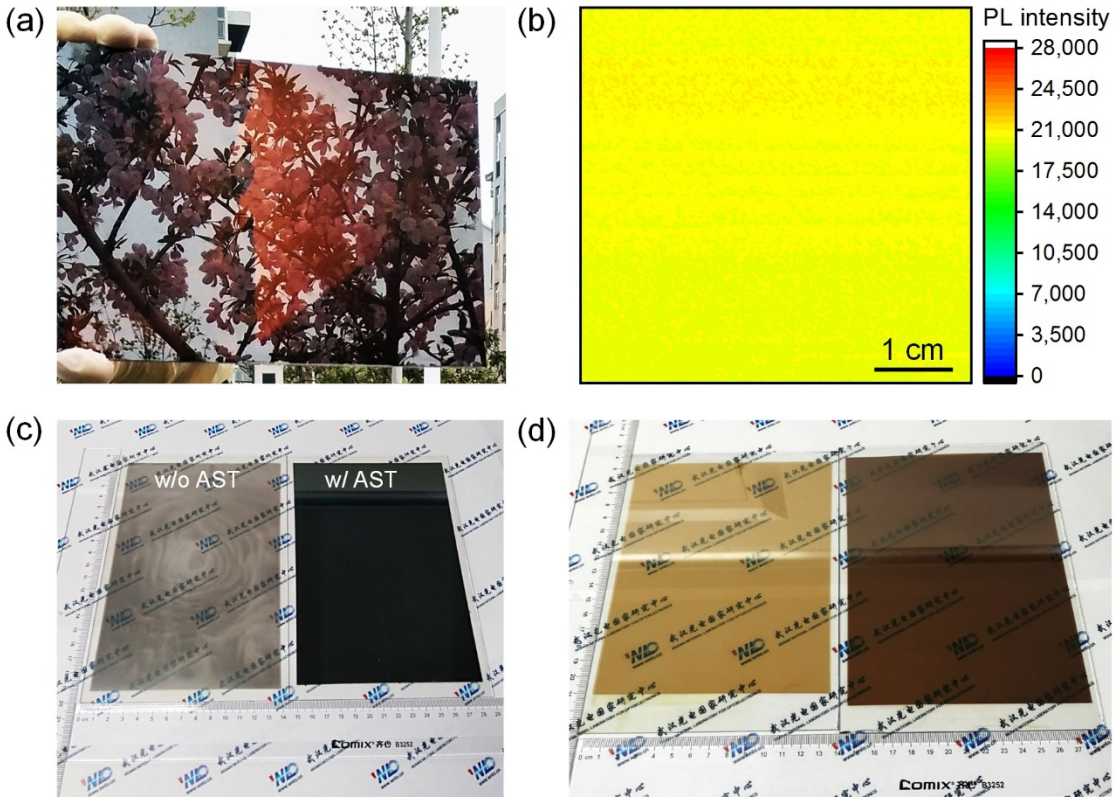

Figure 11. a) The optical image of FACs perovskite film with a size of 14 cm × 20 cm produced by slot-die coating; b) PL mapping of FACs perovskite film with a size of 5 cm × 5 cm; c) Photograph of large-area perovskite film without (w/o) and with (w/) antisolvent (AST) bath post treatment and the followed annealing process; d) The optical image of large-area FACs perovskite film with different thicknesses by adjusting the precursor ink concentration (left is 0.9 M and right is 1.1 M). Reproduced with permission.[21] Copyright 2021, American Association for the Advancement Science.

4.1.5 Spray coating

Spray coating is another widely used technology to deposit perovskite films over large area. Generally, as depicted in **Figure 13**, a spray coating system consists of a nozzle, a gas pump source, and a hotplate. The nozzle is used to disperse tiny liquid droplets on the target substrate and form the wet film. Then, the wet film is annealed by the hotplate to form the fully crystallized perovskite. The film quality and thickness can be controlled by the precursor ink concentration, the spray cycles of precursor solution over the substrate, and the spray speed.

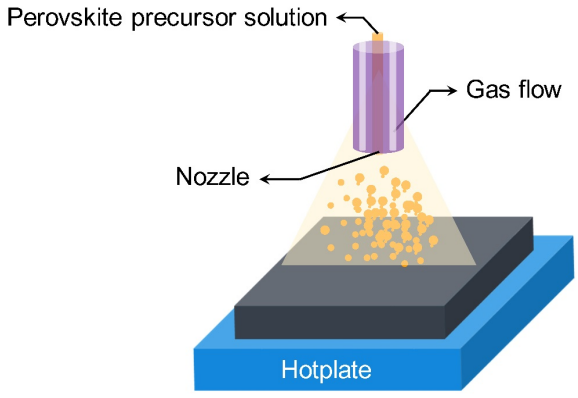

Figure 13. Schematic diagram of spray coating of large-area perovskite films.

However, this technology is limited by the following aspects: (1) the freshly sprayed droplet can dissolve the formed film and affect the coverage of the final film; (2) the scattering of precursor droplets may pollute the fabrication environment. Heo and coauthors fabricated $CH_3NH_3PbI_{3-x}Cl_x$ mixed perovskite film over large area via spray coating technology by

controlling the composition of the solvents of the precursor solution.[53] They found that the inward flux of the spray solution was balanced with the outward flux of the evaporating solvent when the mixed solvent system of DMF and GBL and the large grain size could be achieved (**Figure 14**). In addition, the moistened underlying polycrystalline perovskite film with small crystal grains re-dissolved and merged into larger crystalline grains by recrystallization. Their minimodule achieved an efficiency of 15.5% with an active area of 40 cm^2 as shown in Figure 13e. In addition to the deposition of large-area perovskite films by the one-step method via spray coating, Qi and coauthors developed a two-step method to deposit large-area FA-based perovskite film for minimodule. In their method, PbI_2 is deposited by spray coating, and $FAPb(I_{0.85}Br_{0.15})_3$ perovskite is formed by the reaction PbI_2 with organic ammonium salts via chemical vapor deposition (CVD).[37] Their minimodules showed an efficiency of 14.7% with an active area of 12.0 cm^2.

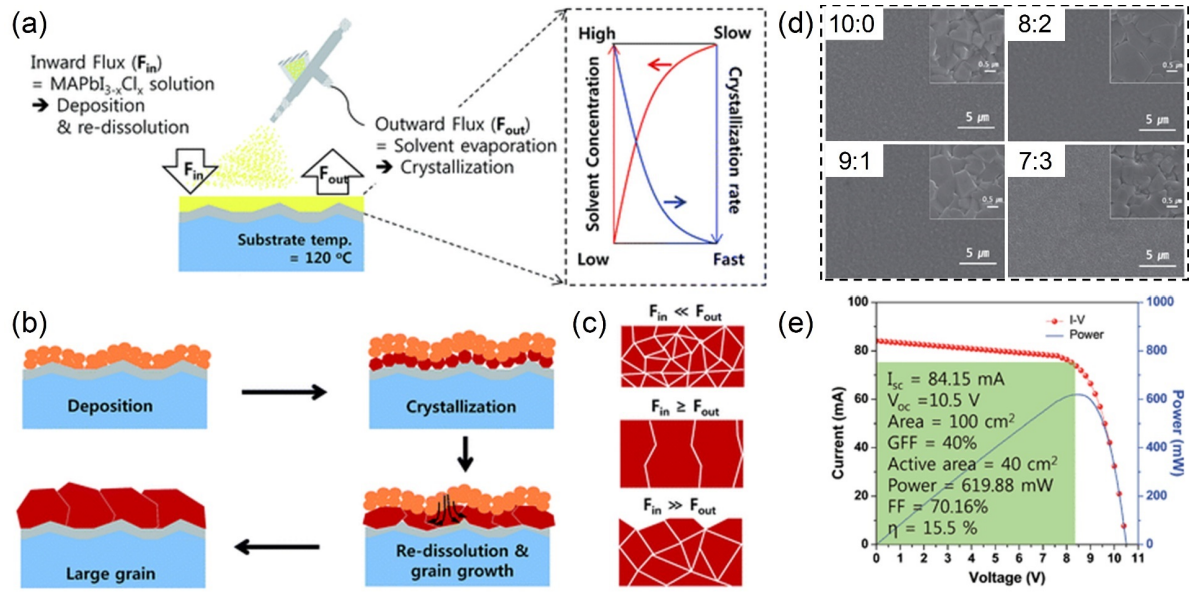

Figure 14. Schematic illustration of a) the proposed mechanism of the spray coating process, b) crystalline grain growth, and c) the morphology diagram of the formed crystalline grains in the perovskite film with respect to the balance between F_{in} and F_{out}. d) the perovskite SEM images spray coated with different ratio of DMF and GBL, e) *I-V* curve of the series module

that perovskite film deposited by spray coating. Reproduced with permission.[53] Copyright 2016, Royal Society of Chemistry.

In the above-mentioned studies, the perovskite film quality and PSM's efficiencies fabricated by solution processing still cannot catch up with that of the lab-scale PSCs prepared by spin-coating. The parameters in doctor blade coating, bar coating, and slot-die coating need to be further optimized to improve film quality, such as perovskite solution composition associated colloid chemistry and wet film drying process. The perovskite crystallization process should also be monitored by some kinds of *in situ* characterization techniques, which will benefit understanding and precise process control.[73]

4.1.6 Vapor-phase methods

Vapor-phase methods are traditional scalable methods to fabricate uniform and compact semiconductor films especially in the fabrication of commercial solar cells such as CdTe. Generally, the vapor-phase method can be classified as physical vapor deposition (PVD) and chemical vapor deposition (CVD). Since 2013, the evaporation deposition method is firstly used to deposit hybrid perovskite film ($MAPbI_{3-x}Cl_x$) for planar PSCs.[74] It is a method that does not need any solvent for the formation of perovskite film, and it exhibits significant advantages in terms of film uniformity over large area. It is not severely constrained by the substrate size. Compared with solution technologies in PSC fabrication, vacuum deposition is beneficial for the fabrication of devices with a stacked or tandem structure, as it can avoid the risk of solvent damage to the underneath deposited layer. Moreover, it is solvent free. However, the device performance still lags behind those fabricated by the solution technology. The main reasons can be ascribed to the following aspects:

(a) It is difficult to form films with an accurate chemical stoichiometric ratio of perovskite composition using vacuum based technologies. Especially, the evaporation of organic ammonium salts such as MAI is complicated due to the difficulty of controlling their

evaporation due to their relatively high vapor pressure.[75-77] In addition, organic ammonium salts such as MAI has shown a relative low sticking coefficient and the tendency to deprotonate into CH_3NH_2 and hydrogen iodide during the evaporation process[78] or decompose to CH_3I and NH_3.[79]

(b) The limited morphology, crystallinity and defect control (*e.g.*, additive and passivation engineering) of the perovskite layer during vacuum based processing make it challenging for vacuum based technologies to achieve deposition of high-quality perovskite films.

Based on above challenges, currently the device performance fabricated by the vacuum vapor-based method is inferior than the device fabricated by the solution processed methods. Mathews and coauthors proved the scalability of thermally co-evaporated $MAPbI_3$ layers for minimodules fabrication.[33] Their minimodules achieved an efficiency of 18.13% with an active area of 21 cm^2.

In addition, full vapor deposition needs high vacuum, which typically requires expensive vacuum equipment and increases the production cost of PSMs. To overcome this issue, Qi and coauthors developed the hybrid CVD (HCVD) method for the fabrication of large-area perovskite film and minimodules, which only requires low-cost pumping equipment.[34, 35, 80-83] For example, they used HCVD to fabricate Cs-FA mixed cation perovskite films across large areas as shown in **Figure 15**.[34] Typically, the inorganic precursor such as PbI_2/CsBr films are first deposited via single-source or multi-source co-evaporation depending on the needs. Then, the prepared film reacts with the organic specie of FAI by HCVD and resulted in large-area films of $Cs_{0.1}FA_{0.9}PbI_{2.9}Br_{0.1}$. Their minimodules achieved an efficiency of 9.34% with a designated area of 91.8 cm^2. Based on the conventional HCVD process that typically needs a relatively long processing time (*e.g.*, several hours), Qi and coauthors recently developed a rapid HCVD (RHCVD) fabrication process by using a rapid thermal process, which significantly reduces the deposition time to less than 10 min.[83] The markedly reduced

deposition time is also found to benefit the formation of high-quality SnO_2 electron-transport layer. Their minimodule with a designated area of 22.4 cm^2 achieved an efficiency of 12.3%, and maintained 90% of the initial efficiency after operation under continuous light illumination for over 800 h. Besides HCVD, the hybrid method combining the solution and the vapor-phase method has also been developed to fabricate minimodules, which helps further reduce the film production cost.[37]

Based on the discussion above, the comparison of the characteristics corresponding to the various deposition methods for depositing large-area perovskite films is summarized in **Table 2**.

Table 2. Comparison of the characteristics corresponding to the various deposition methods for depositing large-area perovskite films.

Deposition method	Whether scalable (> 200 cm^2)	Material waste rate	Film uniformity	Deposition layer	The equipment cost
Spin coating	Yes	High	General	Perovskite, ETL, HTL	Low
Doctor blade coating	Yes	Moderate	Good	Perovskite, ETL, HTL	Low
Bar coating	Yes	Moderate	Good	Perovskite, ETL, HTL	Low
Slot-die coating	Yes	Low	Excellent	Perovskite, ETL, HTL	High
Spray coating	Yes	High	General	Perovskite, ETL, HTL	Low
Vapor deposition	Yes	Low	Excellent	Perovskite, ETL, HTL, Electrode	High

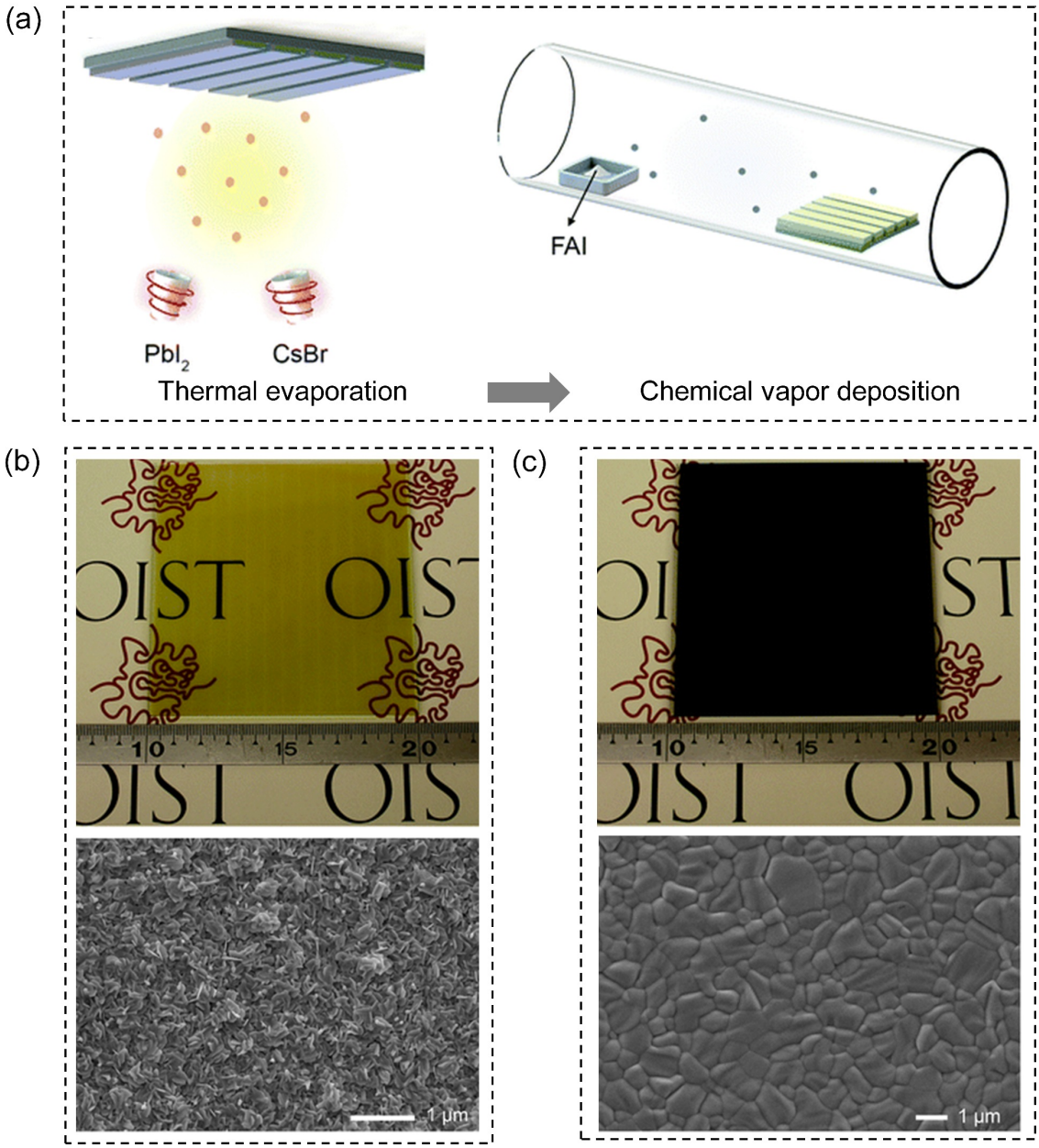

Figure 15. a) Schematic illustration of depositing $Cs_{0.1}FA_{0.9}PbI_{2.9}Br_{0.1}$ perovskite films with the method of HCVD; b) The optical (top) and SEM (bottom) image of a PbI_2/CsBr film deposited by the method of dual-source co-evaporation in vacuum; c) The optical image and SEM image of the final perovskite film after the further reaction with FAI by the process of CVD. Reproduced with permission.[34] Copyright 2019, Royal Society of Chemistry.

4.2 Deposition of charge-transport layers

The fabrication of compact, uniform, and pinhole-free charge transport layers including

electron transport layer (ETL) and hole transporting layer (HTL) over a large area is also important for fabricating high-efficiency and stable PSMs. As for the charge-transport layers, firstly, the selection of suitable charge transport materials with appropriate interfacial energy alignment with the adjacent perovskite light absorber governs the charge extraction at the perovskite/ETL and perovskite/HTL interfaces within the devices. In addition, charge-transport layers should possess full coverage, suitable thickness, and high carrier mobility. In general, charge-transport materials used in PSMs can be divided into organic and inorganic materials. Besides, the processability of charge transport material should also be taken into consideration, such as the deposition of charge-transport layer on perovskite layer should not damage perovskite and the scribing of charge-transport layer during P2 scribing should be easy to form perfect interconnection.

In n-i-p minimodules, TiO_2[26] and SnO_2[11] are the most commonly used materials to construct efficient devices. Soft organic materials such as Spiro-OMeTAD,[84] PTAA,[27, 85] and P3HT[42] are widely used as hole transport materials. In p-i-n minimodules, PCBM[20] or C60[21] are the commonly used electron transport material and PEDOT: PSS[86], PTAA,[27] or NiO_x[21] are usually used as hole transport materials.

The TiO_2 compact layer can be deposited by the scalable solution processing strategy of spray pyrolysis.[26] In addition, the vacuum methods, such as magnetron sputtering[87] or electron-beam evaporation[88] have also been explored. Furthermore, a compact TiO_2 layer can be deposited by low-temperature techniques, such as atomic layer deposition (ALD), which is superior for the fabrication of flexible PSMs.[89] SnO_2 is another representative ETL material used for PSCs, and there are several reasons for replacing TiO_2 with SnO_2 in PSCs: (1) SnO_2 exhibits higher open-circuit voltage (V_{OC}); (2) smaller current density-voltage hysteresis; (3) negligible photocatalytic effect, which is beneficial for the long-term stability of PSCs.[57] The optimized thickness of the SnO_2 layer in PSCs is thinner than that of TiO_2; thus, it is more

challenging to obtain a pinhole-free layer, especially on rough FTO substrates. When SnO_2 is processed at high temperatures, it is usually too crystalline and conductive, and therefore cannot be used as an effective ETL in PSCs. Thus, SnO_2 films are normally deposited with low-temperature ALD technology and a simple post-annealing treatment.[11] Besides, in the fabrication of p-i-n PSCs or minimodule, the commonly used organic-based electron transport materials, such as fullerene (C60) or its derivatives (*i.e.*, PCBM). In general, C60 can be deposited by the method of thermal evaporation,[21, 31] and PCBM is usually deposited by the method of spin coating for PSCs or minimodule fabrication. However, it is greatly restricted by the cost of raw materials. PEDOT: PSS is a kind of hole transport material, which is widely used in organic solar cells and inverted PSCs. However, PEDOT is hygroscopic and tends to absorb moisture from the environment, which is detrimental to the stability of PSCs. Besides, PTAA is another ideal HTL for PSCs fabrication and it can be deposited by the doctor blade coating method.[31] But the wettability of perovskite ink on PTAA is poor, and improving ink wettability is essential. NiO_x is a popular alternative to PEDOT: PSS and PTAA, and it can be deposited using scalable deposition techniques such as spray pyrolysis, atomic layer deposition, and sputtering. However, NiO_x based HTLs are usually annealed at 300−500 °C to increase their crystallinity and conductivity. The high-temperature treatment hinders the use of NiO_x−based HTLs on flexible substrates. Nevertheless, for the development of inverted PSMs on rigid substrates, the inorganic NiO_x is the most promising and ideal HTL candidate regarding the device long-term stability.

Although some progress has been made on the development of charge-transport layers and perovskite layer, most upscaling studies have focused on the scalable deposition of just one or two of the functional layers. Thus, more efforts should be devoted to developing scalable methods to fabricate all functional layers for efficient and stable PSMs.

4.3 Electrode deposition

The most commonly used electrode materials for PSMs are metal and carbon electrodes. The metal electrode is usually deposited by thermal evaporation and the carbon-based electrode is usually deposited by screen printing.[47] Sputtering is currently less investigated for the fabrication of electrodes for PSCs and PSMs. The challenge for this technology to deposit electrodes for PSCs and PSMs is ion bombardment damage on the organic charge-transport layer or even perovskite active layer. For this reason, incorporating a thin inorganic buffer layer (*i.e.*, ZnO or MoO_x) is adopted. On the other hand, sputtering is commonly used for the deposition of transparent conducting oxides (*i.e.*, ITO or aluminum−doped zinc oxide (AZO)), which are used as transparent electrodes in semitransparent or and tandem devices. Moreover, the transparent oxide back electrodes can benefit the device stability due to their compact morphology to isolate the active layer with ambient air and block the leakage of perovskite degradation by-products.

Carbon electrode is a promising candidate for PSCs or PSMs because of cost-effectiveness, chemically stability and environment-friendly properties. The carbon electrode based PSMs developed by Han and coauthors with a device architecture of FTO/m-TiO_2/m-ZrO_2/perovskite/carbon have been demonstrated to show excellent long-term stability.[47] Moreover, this kind of carbon electrode based minimodule is fabricated with screen printing method, which can be easily enlarged to 10 cm × 10 cm level or even larger.

Concerning the reaction between the metal electrode and the migrated halide ions under external stressors, incorporating a barrier electrode beneath the commonly used electrodes has been reported to resolve this problem. For example, the Cr/Au[90] or Bi/Ag electrode[91] scheme has been proposed to suppress the undesired diffusion reaction between the Au or Ag electrode and the perovskite layer. Besides, ion migration can also be suppressed by this strategy. Moreover, the development of the TCO back electrodes with metal grids to make PSM be a

double-sided device is also a promising direction. Besides, either a PSM with series or parallel structure, efficiency loss related to the restricted conductivity of TCO is a concern.

5 Perovskite minimodule stability

5.1 Degradation of perovskites

Degradation of perovskite minimodule can be mainly ascribed to the following aspects: (1) the intrinsic stability of perovskite light absorber layer, the charge transport materials and/or electrodes; (2) the interface and interconnection induced degradation under the operational stress from moisture, light and heat. Taking $MAPbI_3$ as an example, the degradation of $MAPbI_3$ under the above stressors can be analyzed as follows:

(i) Moisture induced degradation. The $MAPbI_3$ hydrate is first formed when the perovskite is exposed to a relative humid condition following the reaction of Equation (1),[92, 93]

$$4CH_3NH_3PbI_3 + 4H_2O \Leftrightarrow (CH_3NH_3)_4PbI_6{\cdot}2H_2O + 3PbI_2 + 2H_2O \quad (1)$$

$MAPbI_3$ hydrate undergoes further decomposition when humidity is high enough according to Equations (2) and (3):

$$(CH_3NH_3)_4PbI_6{\cdot}2H_2O \xrightarrow{H_2O\ (l)} 4CH_3NH_3I\ (aq) + PbI_2\ (s) + 2H_2O\ (l) \quad (2)$$

$$CH_3NH_3I\ (aq) \rightarrow CH_3NH_2\ (aq) + HI\ (aq) \quad (3)$$

Furthermore, if the atmosphere contains oxygen, perovskite undergoes further decomposition following Equation (4):

$$4HI\ (aq) + O_2\ (g) \rightarrow 2I_2\ (s) + 2H_2O\ (l) \quad (4)$$

To reduce the effect of moisture, encapsulation with low water vapor transmission rate is an effective way to improve minimodule stability.[22, 23]

(ii) Light induced degradation.

When exposed to the ultrahigh vacuum (UHV) under light illumination for a long time,[94, 95] $MAPbI_3$ is found to degrade according to Equations (5) and (6):

$$2CH_3NH_3PbI_3 + h\nu \xrightarrow{UHV} CH_3I\ (s) + NH_3\ (g) + 2PbI_2\ (s) + HI\ (g) + CH_3NH_2\ (g) \quad (5)$$

$$PbI_2\ (s) + h\nu \xrightarrow{UHV} Pb\ (s) + I_2\ (g) \quad (6)$$

Light induced degradation of $MAPbI_3$ is irreversible, making $MAPbI_3$ unable to pass the harsh stability test for practical application. The degradation is severe when a device is illuminated under a strong light, especially ultraviolet (UV) light because of its high energy.[95] Moreover, when perovskite is exposed to an atmosphere containing O_2, photo-generated electrons on the surface of the perovskite film react with O_2 molecules according to Equation 7-8:[96]

$$CH_3NH_3PbI_3 \xrightarrow{Light} CH_3NH_3PbI_3* \quad (7)$$

$$O_2 \xrightarrow{CH_3NH_3PbI_3*} O_2^{*-} \quad (8)$$

Furthermore, the perovskite decomposition occurs according to Equation (9):[97]

$$4CH_3NH_3PbI_3^{*} + O_2^{*-} \rightarrow 4CH_3NH_2 + 4PbI_2 + 2I_2 + 2H_2O \quad (9)$$

(iii) Heat induced degradation

$MAPbI_3$ perovskite is unstable under relatively high temperatures (e.g., 85 °C). This is because the formulation energy of $MAPbI_3$ is as low as ~ 0.11 eV,[98] and the bond energy values for C−N and N−H in MA^+ are also low. It is thus easy to break the chemical bonds leading to perovskite structure collapse according to Equations (10) and (11):[66]

$$CH_3NH_3PbI_3 \xrightarrow{\Delta} CH_3NH_2 + PbI_2 + HI \quad (10)$$

$$CH_3NH_3 \xrightarrow{\Delta} CH_3I\ (s) + NH_3\ (g) \quad (11)$$

Recently, FA based perovskites have attracted much attention due to their better chemical (thermal) stability and resistance to evaporation compared to the MA based perovskites.[99] FACs perovskites have been demonstrated to be stable even under the harsh light-heating

stability test condition.[67, 100, 101] Qi and coauthors performed a systematic study on the degradation of FA based perovskites follows Equations 12-14:[99]

$$FAPbX_3 \leftrightarrow PbX_2\,(s)+FA\,(g)+HX\,(g) \quad (12)$$

$$FA \leftrightarrow HCN\,(g)+NH_3\,(g) \quad (13)$$

$$3FA \rightarrow C_3H_3N_3\,(g)+3NH_3\,(g) \quad (14)$$

It is also found that the formation of sym-triazine ($C_3H_3N_3$), FA, and hydrogen cyanide (HCN) is highly dependent on the temperature during their thermogravimetry-mass spectrometry analysis. Under high vacuum test condition, irreversible reaction (14) only occurs at temperatures above 95 °C. This temperature is well above the typical working temperature range of PV applications. Besides, this reaction requires three FA molecules at the same time and involves a complex condensation reaction, which is difficult to occur in highly crystallized perovskite bulk films. In addition, Reactions (12) and (13) are reversible, and it is possible to react back to form FA molecules or cations, making these two reactions effectively suppressed by robust encapsulation.[102] Thus, FA-based perovskites are a promising candidate for the future development of PSMs.

Besides the intrinsic degradation of perovskites, the module structure should also be taken into consideration regarding device long-term stability as discussed in the module architecture part. The possible degradation in a module includes the following aspects:[12, 20] (1) the direct contact of perovskite with the metal electrode induces the reaction of metal with perovskite; (2) the unconfined degradation of perovskites at open interconnection lines P3; (3) the vertical interdiffusion of metal electrode and out-release of perovskite degradation by-products.

In practical applications of PSMs, the aging of a module occurs by illumination with natural sunlight and weather conditions, which makes the degradation of PSMs complex. For example, the degradation could be substantially accelerated under light and heat induced degradation (LeTID) condition or potential induced degradation condition (PID). Some other

conditions, such as local hot spots,[30] partial shading[28] of PSMs should also be considered to study the degradation of PSMs. In some cases, the hot-spot effect is a more tricky problem, because the hot-spot's temporary temperature could reach as high as >150 °C.[103] The shading effect in series modules also can lead to very high temperatures at the shaded subcells area. Even for FACs perovskites, which are likely the most stable absorber in high efficiency PSCs and PSMs, they also require effective barriers and encapsulation to protect them from degradation under real-working conditions.[22, 23]

5.2 Recommendations for minimodule stability testing

The commercialization of perovskite PV technology is upcoming. However, stability issues impede its commercialization. So far, there are no standard stability test protocols established specifically for PSMs. Some long-term stability test protocols for other photovoltaic modules such as crystalline silicon solar modules (IEC-61215, **Figure 16**) and organic photovoltaic cells (International Summit on Organic PV stability (ISOS) protocols) have been recommended for PSMs.[104-107] The commonly used damp-heat aging (85 °C and 85% RH, 1000 h), thermal cycling (−40 °C to 85 °C, 200 cycles), light-soaking aging (MPP at 1 sun and 50 °C ± 10 °C), and UV pre-conditioning (15 kWh m^{-2} at 60 °C ± 5 °C) tests are the basic requirements for the practical use of PSMs.[108] But it must be admitted that the intrinsic stability of perovskites differs significantly from other photovoltaic materials such as silicon, which is intrinsically stable under light, heat and bias. Thus, passing IEC 61215 may be the minimum requirement for PSMs. Protocols containing the factors of light, LETID, PID, partial shade stress, and mechanical shock tests should be built for the stability evaluation of PSMs. Moreover, it is also useful to perform systematic tests such as outdoor stability,[109] light cycling and solar-thermal cycling etc.[107]

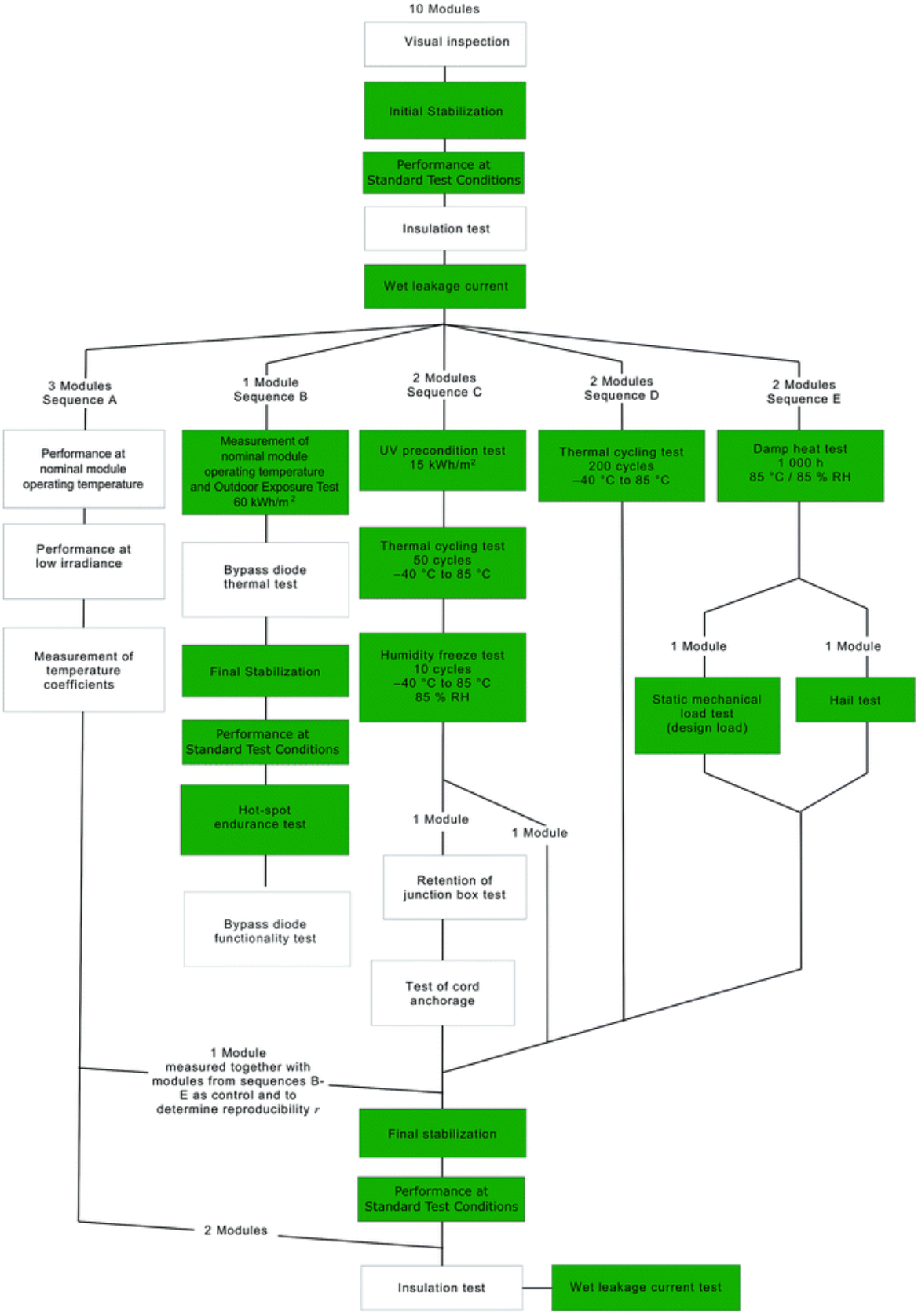

Figure 16. Full test requirements for thin-film PV modules based on IEC 61215. Reproduced with permission.[105] Copyright 2019, Royal Society of Chemistry.

In the future, regarding the minimodule stability study, it is encouraged to re-define for the test of PSMs considering the intrinsic stability of metal halide perovskite materials. On the one hand, the accelerated aging tests are recommended to involve the standard light illumination, maximum power point tracking (MPPT), and heat stressor. The test temperature can be increased to 65 ºC or even higher to 85 ºC. More systematic tests are also recommended such as outdoor stability, thermal cycling, light cycling and solar-thermal cycling, etc.[107] On the other hand, the applications such as photovoltaic glass and indoor PV are also expected to promote the commercialization of this emerging photovoltaic technology. In these applications, the stability tests could be less stringent than outdoor applications.

5.3 Stability improvement strategies for minimodule

Tremendous efforts have been devoted to improving the module stability, but it must be admitted that the intrinsic-determined stability of perovskites is not like the other photovoltaic materials such as silicon, which is intrinsically stable under light, heat and bias. The stability of PSMs is still on the way.

Many strategies have been developed to improve the stability of PSCs.[106, 110] Transferring the accumulated successful experiences in PSCs to PSMs is urgent to improve PSM stability. Similar to the PSC instability issue, the intrinsic instability of perovskite material used for the active layer should also be of primary importance. Compared to the commonly used MA-based perovskite with poor thermal stability, FA-based perovskites incorporated with Cs anion or Br ion exhibit higher intrinsic stability under moisture, light and heat stress, making FACs perovskites to be one of the most promising compositions for high-efficiency and stable PSMs. Besides, 2D perovskite[111, 112] and inorganic perovskite[113-115] with improved moisture and thermal stability are also potential candidates. Besides organic-inorganic hybrid perovskites, the development of all-inorganic perovskite based solar minimodules is another promising direction to fabricate efficient and stable PSMs. The first inorganic perovskite solar minimodule

was reported by Mai and coauthors in 2020.[116] The authors used a ZnO@C60 electron transporting bilayer with tris (pentafluorophenyl) borane and $LiClO_4$ to reduce charge recombination and increase film conductivity. Based on above strategy, they achieved a minimodule PCE of 10.79% and 12.19% (active area = 10.92 cm^2) under forward scan and reverse scan, respectively, with a device structure of FTO/NiO_x/$CsPbI_2Br$/ZnO@C60/Ag. Moreover, the fabricated inorganic minimodule kept about 86.5% of its initial PCE after being stored for 75 days in dry N_2 atmosphere without any encapsulation. Recently, Im and coauthors fabricated an inorganic perovskite solar minimodule and achieved an impressive module efficiency of 13.82% (aperture area = 112 cm^2) with a module structure of FTO/$cTiO_2$/$CsPbI_{3-x}Br_x$/PTAA/Au. [117] Moreover, the unencapsulated minimodule maintained 90.7% of its initial efficiency after aging under 1 sun illumination, in dry N_2 atmosphere, at room temperature and under open circuit conditions for 1000 h. However, the reports about perovskite solar minimodules based on inorganic perovskite materials are relatively scarce due to the difficulty in fabricating inorganic perovskite films via the scalable method. **Table 3** summarizes the recent progress of the structure, performance and stability of inorganic perovskite minimodules.

Table 3. Summary of perovskite solar minimodules based on the inorganic perovskites.

Module structure	PCE (%)	V_{OC} (V)	J_{SC} (mA cm^{-2})	FF (%)	Number of cells	GFF (%)	Area (cm^2)	Perovskite film deposition method	Module stability	Ref.
FTO/NiO_x/$CsPbI_2Br$ /ZnO@C60/Ag	10.79[ac]	4.43	3.77[ac]	60.5	4	75	10.92[ac]	"Quasi-curved" heating	N_2, storage, unencapsulated PSM, $T_{86.5}$=75 days	[116]
FTO/ZnO-ZnS/m-TiO_2/$CsPbI_3$/ spiro-OMeTAD/Au	11.25[ac]	4.00	4.01	70.32	4	N/A	8[ac]	Spin coating	1 sun, MPP tracking, 60% RH, encapsulated PSM, $T_{95.2}$=500 h	[118]
	10.54[ac]	3.86	3.98	68.60		N/A		Blade coating		
FTO/cTiO_2/$CsPbI_{3-x}Br_x$ /PTAA/Au	13.82[ap]	7.64	2.51	72.09	7	N/A	112[ap]	Spray coating	1 sun, N_2, room temperature, open circuit, unencapsulated PSM, $T_{90.7}$=1000 h	[117]
FTO/c-TiO_2/$CsPbI_2Br$/P3HT/Au	11.58[ac]	3.54	4.60	71.09	3	98	25[ac]	Spin coating	1 sun, at 100 °C, MPP tracking, 25% RH, $T_{91.2}$=1000 h	[119]
FTO/c-TiO_2/$CsPbI_3$/CITTIN-2F/Au	10.98[ac]	9.36	1.96	60	9	N/A	27[ac]	Spin coating	N/A	[120]

Beyond that, other strategies including composition engineering, additive or passivation engineering are also suggested to improve perovskite stability.[106]

Besides the stability of perovskites, the development of stable interface layer and electrode is also important to improve module stability.[121] For the electron transport materials used in n-i-p structured devices, SnO_2 is generally used as ETL to avoid the unwanted photocatalytic effect of TiO_2 and improve the device stability. For the commonly used HTL of spiro-OMeTAD, lithium bis (trifluoromethylsulfonyl) imide (LiTFSI) is a widely used dopant to enhance the conductivity and hole mobility. However, the Li^+ ions are highly mobile and hygroscopic, and can migrate across the device under operational stress, resulting in undesired hysteresis and moisture-induced degradation.[122] For this issue, stable dopant-free organic HTLs and inorganic HTLs are regarded as potential candidates.[123] In addition to n-i-p PSCs, p-i-n devices usually show better stability due to the employment of intrinsic stable interface layers such as the inorganic HTL material of NiO_x and stable ETL of C_{60}. For example, McGehee and coauthors fabricated planar p-i-n PSCs based on NiO HTL and their encapsulated devices passed the IEC 61646 temperature cycling test.[124] Besides, they found that the fracture energy increased two times after 250 standardized temperature cycles and four times after laminating an encapsulant on top of the device. Moreover, they also developed a glass-glass encapsulation strategy for p-i-n PSCs to pass the standard IEC 61646 damp heat and thermal cycling tests.[125] In addition, Snaith and coauthors reported small size p-i-n PSCs based on the FACs perovskite with additional piperidinium salt passivation.[100] Their devices can withstand the high temperature stress of 60 ºC and 85 ºC during operation under continuous light illumination. These promising findings suggest that PSCs show a great potential to pass the toughest stability testing against LeTID. These successful examples can thus serve as steppingstones to inspire researchers to transfer these PSCs stability improvement strategies into large-area PSMs. For example, Qi and coworkers developed a holistic interface stabilization strategy by modifying

all the relevant layers and interfaces, namely the perovskite layer, charge transporting layers and device encapsulation, and boosting stability and efficiency of PSMs with an aperture area efficiency over 16% and operation stability over 2000 h.[13]

In addition to the intrinsic stability of perovskite, interface layers, electrode and device engineering for the design of efficient and stable minimodule, the encapsulation strategies should also be considered to further provide mechanical protection and improve the lifetime of the minimodule for practical application. Currently, the encapsulation of perovskite minimodule can be divided into three categories: (1) thin film encapsulation; (2) cover-glass encapsulation; (3) hybrid encapsulation (combining the thin-film and cover-glass encapsulation). With regard to the thin film encapsulation, firstly, the inorganic oxide film (Al_2O_3 and SnO_2)[126, 127] deposited by ALD technology is widely reported. Secondly, organic film encapsulation materials are also reported, like polydimethylsiloxane (PDMS) and parylene film.[128] For the cover-glass encapsulation, the selection of hot-melt film or encapsulation glue (*i.e.*, UV glue) is critical for the effective encapsulation strategy without significant performance loss. For the hot-melt film along the edge of the cover glass for the encapsulation process, the encapsulation mainly finished by the laminating machine, and the hot-pressing temperature for the encapsulation film must be matched with the selected perovskite materials decomposition temperature.[129] The encapsulation glue release content cannot be harmful to the stability of perovskite associate with the interface layers. The hybrid encapsulation is the stack of the above film and cover-glass encapsulation to provide strong protection for perovskite minimodule.[12]

Furthermore, Ahmadi and coauthors introduced a thermally adjusted phase change material into a polymer encapsulation layer to avoid the moisture diffusion, rapid temperature fluctuation, and undesired crystalline phase change of the perovskite layer in the PSCs under the operation condition.[130] As a result, a 2-year stable device was achieved.

In addition to isolating the moisture, oxygen and withstand the thermal stress, especially the cover encapsulation, it can also protect the module device from the practical climate atmosphere of dust, windstorm and rain destroy. Moreover, it can also reduce the leakage of Pb from Pb-based devices and prevent environmental pollution.[131] Lastly, encapsulation plays an important role in perovskite PV technology toward its commercialization.

6 Conclusion and Outlook

In this review, the perspective and recent advances on the development of perovskite solar minimodule are presented. To construct highly efficient and stable PSMs, proper minimodule configuration design is the first key factor. Series modules have achieved tremendous advances in stability and efficiency. Recently, parallel modules have attracted more attention due to their unique module structure considering the non-contact between the metal electrode and the perovskite layer in the interconnection channel, and its advantages against shading effect and partial failure.

Furthermore, the deposition of uniform perovskite and the selective charge transport layers and electrode by the reliable scalable fabrication technology is another key factor. Doctor blade coating and slot-die coating are the most promising technologies compatible with the industrial production line for the fabrication of high-quality perovskite film over hundreds of square centimeters. To date, the commonly used technology for the deposition of charge transport layers is spray pyrolysis, thermal evaporation, blade coating, or slot-die coating. The promising screen printing and evaporation technologies are developed for the fabrication of carbon or metal electrode materials.

Apart from the scalable fabrication process, the stability of PSMs issue is another important factor. To improve PSM's stability, the development of intrinsic stable perovskite, interface layer, and electrode is important. Besides, developing effective barrier and encapsulation methods is also essential to further improve the module stability and decrease the

lead leakage for the practical application of PSMs. The module stability evaluation protocols are also important, and LeTID and PID are recommended for future module stability studies.

To further improve the stability of PSMs, it is desirable to transfer the successful strategies in high efficiency PSCs to PSMs. Considering that perovskite tandem solar cells[132, 133] have achieved very high efficiencies, it is thus promising to develop perovskite tandem modules in the future. To broaden the application of PSMs, the development of semitransparent[134] or flexible[135-137] perovskite minimodule is another promising direction to promote the industrialization process of perovskite PV technology. Semitransparent minimodule can be applied in BIPV or tandem devices. Flexible perovskite minimodule can be integrated into the self-powered smartwatch or other intelligent optoelectronic equipment.

Although encouraging progress has been achieved for high efficiency and stable minimodules, the practical application of this emerging PV technology is still on the way. Various applications can be explored for perovskite PV technology in the near future.

Acknowledgments

Z. Y. and Z. L. contributed equally to this work. Z. L. acknowledges the funding support from the National Natural Science Foundation of China (52002140), Fundamental Research Funds for the Central Universities (2020kfyXJJS008), Natural Science Foundation of Hubei Province (ZRMS2020001132). Y. B. Q. acknowledges the support from the Energy Materials and Surface Sciences Unit of the Okinawa Institute of Science and Technology Graduate University.

References

[1] M. A. Green, A. Ho-Baillie, H. J. Snaith, *Nat. Photonics* **2014**, *8*, 506.

[2] Best research-cell efficiencies. https://www.nrel.gov/pv/assets/pdfs/best-research-cell-efficiencies.20200925.pdf.

[3] N.-G. Park, K. Zhu, *Nat. Rev. Mater.* **2020**, *5*, 333.

[4] M. A. Green, E. D. Dunlop, J. Hohl-Ebinger, M. Yoshita, N. Kopidakis, X. Hao. *Prog Photovolt Res Appl.* **2021**, *29*, 657.

[5] Z. Yang, B. H. Babu, S. Wu, T. Liu, S. Fang, Z. Xiong, L. Han, W. Chen, *Sol. RRL* **2019**, *4*, 1900257.

[6] D. H. Kim, J. B. Whitaker, Z. Li, M. F. A. M. van Hest, K. Zhu, *Joule* **2018**, *2*, 1437.

[7] M. A. Green, K. Emery, Y. Hishikawa, W. Warta, E. D. Dunlop, D. H. Levi, A. W. Y. Ho-Baillie, *Prog. Photovolt. Res. Appl.* **2017**, *25*, 3.

[8] Z. Li, T. R. Klein, D. H. Kim, M. Yang, J. J. Berry, M. F. A. M. van Hest, K. Zhu, *Nat. Rev. Mater.* **2018**, *3*, 18017.

[9] Y. Rong, Y. Ming, W. Ji, D. Li, A. Mei, Y. Hu, H. Han, *J. Phys. Chem. Lett.* **2018**, *9*, 2707.

[10] M. Yang, D. H. Kim, T. Klein, Z. Li, M. O. Reese, B. Tremolet de Villers, J. Berry, M. F. A. M. van Hest, K. Zhu, *ACS Energy Lett.* **2018**, *3*, 322.

[11] L. Qiu, Z. Liu, L. K. Ono, Y. Jiang, D.-Y. Son, Z. Hawash, S. He, Y. B. Qi, *Adv. Funct. Mater.* **2018**, *29*, 1806779.

[12] Z. Liu, L. Qiu, L. K. Ono, S. He, Z. Hu, M. Jiang, G. Tong, Z. Wu, Y. Jiang, D.-Y. Son, Y. Dang, S. Kazaoui, Y. B. Qi, *Nat. Energy* **2020**, *5*, 596.

[13] L. Gao, L. Chen, S. Huang, X. Li, G. Yang, *ACS Appl. Energy Mater.* **2019**, *2*, 3851.

[14] S. Moon, J. Yum, L. Löfgren, A. Walter, L. Sansonnens, M. Benkhaira, S. Nicolay, J. Bailat, C. Ballif, *IEEE J. Photovoltaics* **2015**, *5*, 1087.

[15] A. L. Palma, F. Matteocci, A. Agresti, S. Pescetelli, E. Calabrò, L. Vesce, S. Christiansen, M. Schmidt, A. D. Carlo, *IEEE J. Photovoltaics* **2017**, *7*, 1674.

[16] L. Rakocevic, R. Gehlhaar, T. Merckx, W. Qiu, U. W. Paetzold, H. Fledderus, J. Poortmans, *IEEE J. Photovoltaics* **2017**, *7*, 404.

[17] G. Mincuzzi, A. L. Palma, A. Di Carlo, T. M. Brown, *ChemElectroChem* **2016**, *3*, 9.

[18] A. L. Palma, *Sol. RRL* **2020**, *4*, 1900432.

[19] L. Rakocevic, G. Schöpe, B. Turan, J. Genoe, T. Aernouts, S. Haas, R. Gehlhaar, J. Poortmans, *Prog. Photovoltaics Res. Appl.* **2020**, *28*, 1120.

[20] E. Bi, W. Tang, H. Chen, Y. Wang, J. Barbaud, T. Wu, W. Kong, P. Tu, H. Zhu, X. Zeng, J. He, S. Kan, X. Yang, M. Grätzel, L. Han, *Joule* **2019**, *3*, 2748.

[21] Z. Yang, W. Zhang, S. Wu, H. Zhu, Z. Liu, Z. Liu, Z. Jiang, R. Chen, J. Zhou, Q. Lu, Z. Xiao, L. Shi, H. Chen, L. K. Ono, S. Zhang, Y. Zhang, Y. B. Qi, L. Han, W. Chen, *Sci. Adv.* **2021**, *7*, eabg3749.

[22] S. Zhang, Z. Liu, W. Zhang, Z. Jiang, W. Chen, R. Chen, Y. Huang, Z. Yang, Y. Zhang, L. Han, W. Chen, *Adv. Energy Mater.* **2020**, *10*, 2001610.

[23] Q. Lu, Z. Yang, X. Meng, Y. Yue, M. A. Ahmad, W. Zhang, S. Zhang, Y. Zhang, Z. Liu, W. Chen, *Adv. Funct. Mater.* **2021**, *31*, 2100151.

[24] http://www.utmolight.com/20492/117028.html.

[25] http://www.microquanta.com/newsinfo/77699E79BBC5D633/.

[26] M. Yang, Z. Li, M. O. Reese, O. G. Reid, D. H. Kim, S. Siol, T. R. Klein, Y. Yan, J. J. Berry, M. F. A. M. van Hest, K. Zhu, *Nat. Energy* **2017**, *2*, 17038.

[27] Y. Deng, X. Zheng, Y. Bai, Q. Wang, J. Zhao, J. Huang, *Nat. Energy* **2018**, *3*, 560.

[28] Y. Deng, C. H. Van Brackle, X. Dai, J. Zhao, B. Chen, J. Huang, *Sci. Adv.* **2019**, *5*, eaax7537.

[29] H. Chen, F. Ye, W. Tang, J. He, M. Yin, Y. Wang, F. Xie, E. Bi, X. Yang, M. Gratzel, L. Han, *Nature* **2017**, *550*, 92.

[30] K. Li, J. Xiao, X. Yu, T. Bu, T. Li, X. Deng, S. Liu, J. Wang, Z. Ku, J. Zhong, F. Huang, Z. Zhong, Y. Peng, W. Li, Y. Cheng, *ACS Appl. Energy Mater.* **2018**, *1*, 3565.

[31] Y. Deng, Z. Ni, A. F. Palmstrom, J. Zhao, S. Xu, C. H. Van Brackle, X. Xiao, K. Zhu, J. Huang, *Joule* **2020**, *4*, 1949.

[32] T. Bu, J. Li, H. Li, C. Tian, J. Su, G. Tong, L. K. Ono, C. Wang, Z. Lin, N. Chai, X.-L. Zhang, J. Chang, J. Lu, J. Zhong, W. Huang, Y. Qi, Y.-B. Cheng, F. Huang, *Science* **2021**, *372*,1327.

[33] J. Li, H. Wang, X. Y. Chin, H. A. Dewi, K. Vergeer, T. W. Goh, J. W. M. Lim, J. H. Lew, K. P. Loh, C. Soci, T. C. Sum, H. J. Bolink, N. Mathews, S. Mhaisalkar, A. Bruno, *Joule* **2020**, *4*, 1035.

[34] L. Qiu, S. He, Y. Jiang, D.-Y. Son, L. K. Ono, Z. Liu, T. Kim, T. Bouloumis, S. Kazaoui, Y. B. Qi, *J. Mater. Chem. A* **2019**, *7*, 6920.

[35] Y. Jiang, M. R. Leyden, L. Qiu, S. Wang, L. K. Ono, Z. Wu, E. J. Juarez-Perez, Y. B. Qi, *Adv. Funct. Mater.* **2018**, *28*, 1703835.

[36] Y. Deng, S. Xu, S. Chen, X. Xiao, J. Zhao, J. Huang, *Nat. Energy* **2021**, *6*, 633.

[37] Y. Jiang, M. Remeika, Z. Hu, E. J. Juarez-Perez, L. Qiu, Z. Liu, T. Kim, L. K. Ono, D. Y. Son, Z. Hawash, M. R. Leyden, Z. Wu, L. Meng, J. Hu, Y. B. Qi, *Adv. Energy Mater.* **2019**, *9*, 1803047.

[38] L. Luo, Y. Zhang, N. Chai, X. Deng, J. Zhong, F. Huang, Y. Peng, Y.-B. Cheng, Z. Ku, *J. Mater. Chem. A* **2018**, *6*, 21143.

[39] Z. Liu, L. Qiu, E. J. Juarez-Perez, Z. Hawash, T. Kim, Y. Jiang, Z. Wu, S. R. Raga, L. K. Ono, S. F. Liu, Y. B. Qi, *Nat. Commun.* **2018**, *9*, 3880.

[40] S. Tian, J. Li, S. Li, T. Bu, Y. Mo, S. Wang, W. Li, F. Huang, *Sol. Energy* **2019**, *183*, 386.

[41] T. Bu, J. Li, F. Zheng, W. Chen, X. Wen, Z. Ku, Y. Peng, J. Zhong, Y. B. Cheng, F. Huang, *Nat. Commun.* **2018**, *9*, 4609.

[42] E. H. Jung, N. J. Jeon, E. Y. Park, C. S. Moon, T. J. Shin, T. Y. Yang, J. H. Noh, J. Seo, *Nature* **2019**, *567*, 511.

[43] A. Ren, H. Lai, X. Hao, Z. Tang, H. Xu, B. M. F. Yu Jeco, K. Watanabe, L. Wu, J. Zhang, M. Sugiyama, J. Wu, D. Zhao, *Joule* **2020**, *4*, 1263.

[44] A. Agresti, S. Pescetelli, A. L. Palma, A. E. Del Rio Castillo, D. Konios, G. Kakavelakis, S. Razza, L. Cinà, E. Kymakis, F. Bonaccorso, A. Di Carlo, *ACS Energy Lett.* **2017**, *2*, 279.

[45] A. Agresti, S. Pescetelli, A. L. Palma, B. Martin-Garcia, L. Najafi, S. Bellani, I. Moreels, M. Prato, F. Bonaccorso, A. Di Carlo, *ACS Energy Lett.* **2019**, *4*, 1862.

[46] A. Priyadarshi, L. J. Haur, P. Murray, D. Fu, S. Kulkarni, G. Xing, T. C. Sum, N. Mathews, S. G. Mhaisalkar, *Energy Environ. Sci.* **2016**, *9*, 3687.

[47] Y. Hu, S. Si, A. Mei, Y. Rong, H. Liu, X. Li, H. Han, *Sol. RRL* **2017**, *1*, 1600019.

[48] G. Grancini, C. Roldán-Carmona, I. Zimmermann, E. Mosconi, X. Lee, D. Martineau, S. Narbey, F. Oswald, F. De Angelis, M. Graetzel, M. K. Nazeeruddin, *Nat. Commun.* **2017**, *8*, 15684.

[49] H.-J. Kim, H.-S. Kim, N.-G. Park, *Adv. Energy Sustainability Res.* **2021**, *2*, 2000051.

[50] K. Emery, Photovoltaic calibrations at the National Renewable Energy Laboratory and uncertainty analysis following the ISO 17025 guidelines. **2016**, https://www.nrel.gov/docs/fy17osti/66873.pdf.

[51] J. B. Whitaker, D. H. Kim, Bryon W. Larson, F. Zhang, J. J. Berry, M. F. A. M. van Hest, K. Zhu, *Sustain. Energy Fuels* **2018**, *2*, 2442.

[52] J. G. Tait, S. Manghooli, W. Qiu, L. Rakocevic, L. Kootstra, M. Jaysankar, C. A. Masse de la Huerta, U. W. Paetzold, R. Gehlhaar, D. Cheyns, P. Heremans, J. Poortmans, *J. Mater. Chem. A* **2016**, *4*, 3792.

[53] J. H. Heo, M. H. Lee, M. H. Jang, S. H. Im, *J. Mater. Chem. A* **2016**, *4*, 17636.

[54] L. Qiu, S. He, L. K. Ono, S. Liu, Y. B. Qi, *ACS Energy Lett.* **2019**, *4*, 2147.

[55] J.-H. Im, H.-S. Kim, N.-G. Park, *APL Mater.* **2014**, *2*, 081510.

[56] J. J. Yoo, G. Seo, M. R. Chua, T. G. Park, Y. Lu, F. Rotermund, Y. K. Kim, C. S. Moon, N. J. Jeon, J. P. Correa-Baena, V. Bulovic, S. S. Shin, M. G. Bawendi, J. Seo, *Nature* **2021**, *590*, 587.

[57] T. Bu, X. Liu, J. Li, W. Huang, Z. Wu, F. Huang, Y.-B. Cheng, J. Zhong, *Sol. RRL* **2020**, *4*, 1900263.

[58] C. Wang, G. Tan, X. Luo, J. Li, X. Gao, Y. Mo, X.-L. Zhang, X. Wang, F. Huang, *J. Power Sources* **2020**, *466*, 228321.

[59] Q. Jiang, L. Zhang, H. Wang, X. Yang, J. Meng, H. Liu, Z. Yin, J. Wu, X. Zhang, J. You, *Nat. Energy* **2016**, *1*, 16177.

[60] Q. Jiang, Y. Zhao, X. Zhang, X. Yang, Y. Chen, Z. Chu, Q. Ye, X. Li, Z. Yin, J. You, *Nat. Photonics* **2019**, *1*3, 460.

[61] Z. Xu, Z. Liu, N. Li, G. Tang, G. Zheng, C. Zhu, Y. Chen, L. Wang, Y. Huang, L. Li, N. Zhou, J. Hong, Q. Chen, H. Zhou, *Adv. Mater.* **2019**, *31*, 1900390.

[62] J. X. Zhong, W. Q. Wu, L. Ding, D. B. Kuang, *Energy Environ. Mater.* **2020**, *0*, 1.

[63] F. Guo, S. Qiu, J. Hu, H. Wang, B. Cai, J. Li, X. Yuan, X. Liu, K. Forberich, C. J. Brabec, Y. Mai, *Adv. Sci.* **2019**, *6*, 1901067.

[64] S. Razza, F. Di Giacomo, F. Matteocci, L. Cinà, A. L. Palma, S. Casaluci, P. Cameron, A. D'Epifanio, S. Licoccia, A. Reale, T. M. Brown, A. Di Carlo, *J. Power Sources* **2015**, *277*, 286.

[65] J. Zhang, T. Bu, J. Li, H. Li, Y. Mo, Z. Wu, Y. Liu, X. Zhang, Y.-B. Cheng, F. Huang, *J. Mater. Chem. A* **2020**, *8*, 8447.

[66] E. J. Juarez-Perez, Z. Hawash, S. R. Raga, L. K. Ono, Y. B. Qi, *Energy Environ. Sci.* **2016**, *9*, 3406.

[67] S.-H. Turren-Cruz, A. Hagfeldt, M. Saliba, *Science* **2018**, *362*, 449.

[68] M. A. Green, Y. Hishikawa, E. D. Dunlop, D. H. Levi, J. Hohl-Ebinger, A. W. Y. Ho-Baillie, *Prog. Photovolt. Res. Appl.* **2018**, *26*, 427.

[69] K.-S. Lim, D.-K. Lee, J.-W. Lee, N.-G. Park, *J. Mater. Chem. A* **2020**, *8*, 9345.

[70] D.-K. Lee, K.-S. Lim, J.-W. Lee, N.-G. Park, *J. Mater. Chem. A* **2021**, *9*, 3018.

[71] H. Li, T. Bu, J. Li, Z. Lin, J. Pan, Q. Li, X.-L. Zhang, Z. Ku, Y.-B. Cheng, F. Huang, *ACS Appl. Mater. Interfaces* **2021**, *13*, 18724.

[72] L. Cai, L. Liang, J. Wu, B. Ding, L. Gao, B. Fan, *J. Semicond.* **2017**, *38*, 014006.

[73] H. Hu, Z. Ren, P. W. K. Fong, M. Qin, D. Liu, D. Lei, X. Lu, G. Li, *Adv. Funct. Mater.* **2019**, *29*, 1900092.

[74] M. Liu, M. B. Johnston, H. J. Snaith, *Nature* **2013**, *501*, 395.

[75] R. Swartwout, M. T. Hoerantner, V. Bulović, *Energy Environ. Mater.* **2019**, *2*, 119.

[76] L. K. Ono, S. Wang, Y. Kato, S. R. Raga, Y. B. Qi, *Energy Environ. Sci.* **2014**, *7*, 3989.

[77] S. Wang, L. K. Ono, M. R. Leyden, Y. Kato, S. R. Raga, M. V. Lee, Y. B. Qi, *J. Mater. Chem. A* **2015**, *3*, 14631.

[78] M. J. Bækbo, O. Hansen, I. Chorkendorff, P. C. K. Vesborg, *RSC Adv.* **2018**, *8*, 29899.

[79] A. E. Williams, P. J. Holliman, M. J. Carnie, M. L. Davies, D. A. Worsley, T. M. Watson, *J. Mater. Chem. A* **2014**, *2*, 19338.

[80] M. R. Leyden, L. K. Ono, S. R. Raga, Y. Kato, S. Wang, Y. B. Qi, *J. Mater. Chem. A* **2014**, *2*, 18742.

[81] M. R. Leyden, M. V. Lee, S. R. Raga, Y. B. Qi, *J. Mater. Chem. A* **2015**, *3*, 16097.

[82] M. R. Leyden, Y. Jiang, Y. B. Qi, *J. Mater. Chem. A* **2016**, *4*, 13125.

[83] L. Qiu, S. He, Z. Liu, L. K. Ono, D.-Y. Son, Y. Liu, G. Tong, Y. B. Qi, *J. Mater. Chem. A* **2020**, *8*, 23404.

[84] T. Bu, X. Liu, Y. Zhou, J. Yi, X. Huang, L. Luo, J. Xiao, Z. Ku, Y. Peng, F. Huang, Y.-B. Cheng, J. Zhong, *Energy Environ. Sci.* **2017**, *10*, 2509.

[85] N. Yaghoobi Nia, M. Zendehdel, M. Abdi-Jalebi, L. A. Castriotta, F. U. Kosasih, E. Lamanna, M. M. Abolhasani, Z. Zheng, Z. Andaji-Garmaroudi, K. Asadi, G. Divitini, C. Ducati, R. H. Friend, A. Di Carlo, *Nano Energy* **2021**, *82*, 105685.

[86] J. Seo, S. Park, Y. Chan Kim, N. J. Jeon, J. H. Noh, S. C. Yoon, S. I. Seok, *Energy Environ. Sci.* **2014**, *7*, 2642.

[87] D. Yang, R. Yang, J. Zhang, Z. Yang, S. Liu, C. Li, *Energy Environ. Sci.* **2015**, *8*, 3208.

[88] W. Qiu, U. W. Paetzold, R. Gehlhaar, V. Smirnov, H.-G. Boyen, J. G. Tait, B. Conings, W. Zhang, C. B. Nielsen, I. McCulloch, L. Froyen, P. Heremans, D. Cheyns, *J. Mater. Chem. A* **2015**, *3*, 22824.

[89] F. Di Giacomo, V. Zardetto, A. D'Epifanio, S. Pescetelli, F. Matteocci, S. Razza, A. Di Carlo, S. Licoccia, W. M. M. Kessels, M. Creatore, T. M. Brown, *Adv. Energy Mater.* **2015**, *69*, 15.

[90] K. Domanski, J. P. Correa-Baena, N. Mine, M. K. Nazeeruddin, A. Abate, M. Saliba, W. Tress, A. Hagfeldt, M. Gratzel, *ACS Nano* **2016**, *10*, 6306.

[91] S. Wu, R. Chen, S. Zhang, B. H. Babu, Y. Yue, H. Zhu, Z. Yang, C. Chen, W. Chen, Y. Huang, S. Fang, T. Liu, L. Han, W. Chen, *Nat. Commun.* **2019**, *10*, 1161.

[92] J. A. Christians, P. A. Miranda Herrera, P. V. Kamat, *J. Am. Chem. Soc.* **2015**, *137*, 1530.

[93] M. Wu, N. Ladi, Z. Yi, H. Li, Y. Shen, M. Wang, *Energy Technol.* **2020**, *8*, 1900744.

[94] E. J. Juarez-Perez, L. K. Ono, M. Maeda, Y. Jiang, Z. Hawash, Y. B. Qi, *J. Mater. Chem. A* **2018**, *6*, 9604.

[95] G. Abdelmageed, L. Jewell, K. Hellier, L. Seymour, B. Luo, F. Bridges, J. Z. Zhang, S. Carter, *Appl. Phys. Lett.* **2016**, *109*, 233905.

[96] N. Aristidou, I. Sanchez-Molina, T. Chotchuangchutchaval, M. Brown, L. Martinez, T. Rath, S. A. Haque, *Angew. Chem. Int. Ed.* **2015**, *54*, 8208.

[97] N. Aristidou, C. Eames, I. Sanchez-Molina, X. Bu, J. Kosco, M. S. Islam, S. A. Haque, *Nat. Commun.* **2017,** *8*, 15218.

[98] H. S. Kim, J. Y. Seo, N. G. Park, *ChemSusChem* **2016**, *9*, 2528.

[99] E. J. Juarez-Perez, L. K. Ono, Y. B. Qi, *J. Mater. Chem. A* **2019**, *7*, 16912.

[100] Y.-H. Lin, N. Sakai, P. Da, J. Wu, H. C. Sansom, A. J. Ramadan, S. Mahesh, J. Liu, R. D. J. Oliver, J. Lim, L. Aspitarte, K. Sharma, P. K. Madhu, A. B. Morales-Vilches, P. K. Nayak, S. Bai, F. Gao, C. R. M. Grovenor, M. B. Johnston, J. G. Labram, J. R. Durrant, J. M. Ball, B. Wenger, B. Stannowski, H. J. Snaith, *Science* **2020**, *369*, 96.

[101] S. Bai, P. Da, C. Li, Z. Wang, Z. Yuan, F. Fu, M. Kawecki, X. Liu, N. Sakai, J. T.-W. Wang, S. Huettner, S. Buecheler, M. Fahlman, F. Gao, H. J. Snaith, *Nature* **2019**, *571*, 245.

[102] L. Shi, M. P. Bucknall, T. L. Young, M. Zhang, L. Hu, J. Bing, D. S. Lee, J. Kim, T. Wu, N. Takamure, D. R. McKenzie, S. Huang, M. A. Green, A. W. Y. Ho-Baillie, *Science* **2020**, *368*, eaba2412.

[103] C. C. Boyd, R. Cheacharoen, T. Leijtens, M. D. McGehee, *Chem. Rev.* **2019**, *119*, 3418.

[104] M. Saliba, M. Stolterfoht, C. M. Wolff, D. Neher, A. Abate, *Joule* **2018**, *2*, 1019.

[105] P. Holzhey, M. Saliba, *J. Mater. Chem. A* **2018**, *6*, 21794.

[106] S. He, L. Qiu, L. K. Ono, Y. B. Qi, *Mater. Sci. Eng. R Rep.* **2020**, *140*, 100545.

[107] M. V. Khenkin, E. A. Katz, A. Abate, G. Bardizza, J. J. Berry, C. Brabec, F. Brunetti, V. Bulović, Q. Burlingame, A. Di Carlo, R. Cheacharoen, Y.-B. Cheng, A. Colsmann, S. Cros, K. Domanski, M. Dusza, C. J. Fell, S. R. Forrest, Y. Galagan, D. Di Girolamo, M. Grätzel, A. Hagfeldt, E. von Hauff, H. Hoppe, J. Kettle, H. Köbler, M. S. Leite, S. Liu, Y.-L. Loo, J. M. Luther, C.-Q. Ma, M. Madsen, M. Manceau, M. Matheron, M. McGehee, R. Meitzner, M. K. Nazeeruddin, A. F. Nogueira, Ç. Odabaşı, A. Osherov, N.-G. Park, M. O. Reese, F. De Rossi, M. Saliba, U. S. Schubert, H. J. Snaith, S. D. Stranks, W. Tress, P. A. Troshin, V. Turkovic, S. Veenstra, I. Visoly-Fisher, A. Walsh, T. Watson, H. Xie, R. Yıldırım, S. M. Zakeeruddin, K. Zhu, M. Lira-Cantu, *Nat. Energ* **2020**, *5*, 35.

[108] Y. Hu, Y. Chu, Q. Wang, Z. Zhang, Y. Ming, A. Mei, Y. Rong, H. Han, *Joule* **2019**, 3, 2076.

[109] E. Velilla, F. Jaramillo, I. Mora-Seró, *Nat. Energy* **2021**, *6*, 54.

[110] L. K. Ono, Y. B. Qi, S. Liu, *Joule* **2018**, *2*, 1961.

[111] F. Zhang, H. Lu, J. Tong, J. J. Berry, M. C. Beard, K. Zhu, *Energy Environ. Sci.* **2020**, *13*, 1154.

[112] J. Yan, W. Qiu, G. Wu, P. Heremans, H. Chen, *J. Mater. Chem. A* **2018**, *6*, 11063.

[113] J. Liang, J. Liu, Z. Jin, *Sol. RRL* **2017**, *1*, 1700086.

[114] Q. Tai, K.-C. Tang, F. Yan, *Energy Environ. Sci.* **2019**, *12*, 2375.

[115] W. Chen, X. Li, Y. Li, Y. Li, *Energy Environ. Sci.* **2020**, *13*, 1971.

[116] C. Liu, Y. Yang, C. Zhang, S. Wu, L. Wei, F. Guo, G. M. Arumugam, J. Hu, X. Liu, J. Lin, R. E. I. Schropp, Y. Mai, *Adv. Mater.* **2020**, *32*, 1907361.

[117] J. H. Heo, F. Zhang, C. Xiao, S. J. Heo, J. K. Park, J. J. Berry, K. Zhu, S. H. Im, *Joule* **2021**, *5*, 481.

[118] R. Chen, Y. Hui, B. Wu, Y. Wang, X. Huang, Z. Xu, P. Ruan, W. Zhang, F. Cheng, W. Zhang, J. Yin, J. Li, N. Zheng, *J. Mater. Chem. A* **2020**, *8*, 9597.

[119] J. H. Heo, D. H. Kim, J. K. Park, Y. K. Choi, D. S. Lee, S. H. Im, *ACS Appl. Mater. Interfaces* **2019**, *11*, 43066.

[120] M. K. Nazeeruddin, C. Liu, C. Igci, Y. Yang, O. A. Syzgantseva, M. A. Syzgantseva, K. Rakstys, H. Kanda, N. Shibayama, B. Ding, X. Zhang, V. Jankauskas, Y. Ding, S. Dai, P. Dyson, *Angew. Chem. Int. Ed.* **2021**, DOI: 10.1002/anie.202107774.

[121] Z. Liu, Y. B. Qi, *Mater. Matters* **2021**, *16*, 25.

[122] J. A. Christians, P. Schulz, J. S. Tinkham, T. H. Schloemer, S. P. Harvey, B. J. Tremolet de Villers, A. Sellinger, J. J. Berry, J. M. Luther, *Nat. Energy* **2018**, *3*, 68.

[123] E. Rezaee, X. Liu, Q. Hu, L. Dong, Q. Chen, J.-H. Pan, Z.-X. Xu, *Sol. RRL* **2018**, *2*, 1800200.

[124] R. Cheacharoen, N. Rolston, D. Harwood, K. A. Bush, R. H. Dauskardt, M. D. McGehee, *Energy Environ. Sci.* **2018**, *11*, 144.

[125] R. Cheacharoen, C. C. Boyd, G. F. Burkhard, T. Leijtens, J. A. Raiford, K. A. Bush, S. F. Bent, M. D. McGehee, *Sustain. Energy Fuels* **2018**, *2*, 2398.

[126] K. O. Brinkmann, J. Zhao, N. Pourdavoud, T. Becker, T. Hu, S. Olthof, K. Meerholz, L. Hoffmann, T. Gahlmann, R. Heiderhoff, M. F. Oszajca, N. A. Luechinger, D. Rogalla, Y. Chen, B. Cheng, T. Riedl, *Nat. Commun.* **2017**, *8*, 13938.

[127] R. Singh, S. Ghosh, A. S. Subbiah, N. Mahuli, S. K. Sarkar, *Sol. Energy Mater. Sol. Cells* **2020**, *205*, 110289.

[128] Z. Liu, B. Sun, T. Shi, Z. Tang, G. Liao, *J. Mater. Chem. A* **2016**, *4*, 10700.

[129] Z. Fu, M. Xu, Y. Sheng, Z. Yan, J. Meng, C. Tong, D. Li, Z. Wan, Y. Ming, A. Mei, Y. Hu, Y. Rong, H. Han, *Adv. Funct. Mater.* **2019**, *29*, 1809129.

[130] N. Mansour Rezaei Fumani, F. Arabpour Roghabadi, M. Alidaei, S. M. Sadrameli, V. Ahmadi, F. Najafi, *ACS Omega* **2020**, *5*, 7106.

[131] Y. Jiang, L. Qiu, E. J. Juarez-Perez, L. K. Ono, Z. Hu, Z. Liu, Z. Wu, L. Meng, Q. Wang, Y. B. Qi, *Nat. Energy* **2019**, *4*, 585.

[132] A. Al-Ashouri, E. Köhnen, B. Li, A. Magomedov, H. Hempel, P. Caprioglio, J. A. Márquez, A. B. Morales Vilches, E. Kasparavicius, J. A. Smith, N. Phung, D. Menzel, M. Grischek, L. Kegelmann, D. Skroblin, C. Gollwitzer, T. Malinauskas, M. Jošt, G. Matič, B. Rech, R. Schlatmann, M. Topič, L. Korte, A. Abate, B. Stannowski, D. Neher, M. Stolterfoht, T. Unold, V. Getautis, S. Albrecht, *Science* **2020**, *370*, 1300.

[133] K. Xiao, R. Lin, Q. Han, Y. Hou, Z. Qin, H. T. Nguyen, J. Wen, M. Wei, V. Yeddu, M. I. Saidaminov, Y. Gao, X. Luo, Y. Wang, H. Gao, C. Zhang, J. Xu, J. Zhu, E. H. Sargent, H. Tan, *Nat. Energy* **2020**, *5*, 870.

[134] H.-C. Kwon, S. Ma, S.-C. Yun, G. Jang, H. Yang, J. Moon, *J. Mater. Chem. A* **2020**, *8*, 1457.

[135] J. Chung, S. S. Shin, K. Hwang, G. Kim, K. W. Kim, D. S. Lee, W. Kim, B. S. Ma, Y.-K. Kim, T.-S. Kim, J. Seo, *Energy Environ. Sci.* **2020**, *13*, 4854.

[136] X. Hu, Z. Huang, F. Li, M. Su, Z. Huang, Z. Zhao, Z. Cai, X. Yang, X. Meng, P. Li, Y. Wang, M. Li, Y. Chen, Y. Song, *Energy Environ. Sci.* **2018**, *12*, 979.

[137] X. Meng, Z. Cai, Y. Zhang, X. Hu, Z. Xing, Z. Huang, Z. Huang, Y. Cui, T. Hu, M. Su, X. Liao, L. Zhang, F. Wang, Y. Song, Y. Chen, *Nat. Commun.* **2020**, *11*, 3016.

Biographies

Zhichun Yang obtained his B.S. in physics in 2014 from Yun Cheng University, China, and his M.S. in condensed matter physics in 2017 at Huazhong University of Science and Technology, China. He is currently a Ph. D. candidate in Wuhan National Laboratory for Optoelectronics of Huazhong University of Science and Technology. His research mainly focuses on large-area perovskite solar cells and modules.

Zonghao Liu received his B.Sc. in 2011 and Ph.D. in 2016 from Huazhong University of Science and Technology (HUST), China. He was a visiting student in University of California, Los Angeles, USA, in 2015. From 2016 to 2017, he was a research assistant in Peking University, China. From 2017–2019, he worked as a postdoctoral scholar at Okinawa Institute of Science and Technology Graduate University in Japan. He is currently an associate professor in Wuhan National Laboratory for Optoelectronics of HUST. His current research focuses on optoelectronics devices based on inorganic/organic perovskites, especially on perovskite solar cells.

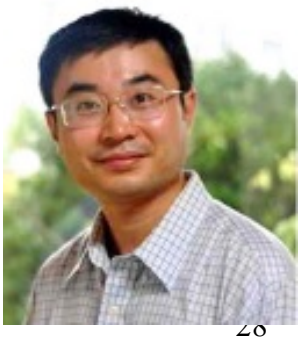

Yabing Qi is Professor and Unit Director of Energy Materials and Surface Sciences Unit at Okinawa Institute of Science and Technology Graduate University in Japan, and a Fellow of the Royal Society of Chemistry. He received his B.S., M.Phil., and Ph.D. from Nanjing University, Hong Kong University of Science and Technology, and UC Berkeley, respectively. His research interests include surface / interface sciences, perovskite solar cells, lithium ion batteries, organic electronics, energy materials and devices (https://groups.oist.jp/emssu).

This article reviews the research progress on metal halide perovskite solar minimodules and their improvements in efficiency and stability.

Zhichun Yang, Zonghao Liu*, Vahid Ahmadi, Wei Chen, Yabing Qi*

Title

Recent Progress on Metal Halide Perovskite Solar Minimodules

ToC figure